COUPLED THERMOMECHANICAL ANALYSIS OF CONCRETE
HARDENING

A THESIS SUBMITTED TO
THE GRADUATE SCHOOL OF NATURAL AND APPLIED SCIENCES
OF
MIDDLE EAST TECHNICAL UNIVERSITY

BY

HALİL İBRAHİM ANDİÇ

IN PARTIAL FULFILLMENT OF THE REQUIREMENTS
FOR
THE DEGREE OF MASTER OF SCIENCE
IN
CIVIL ENGINEERING

FEBRUARY 2015

Approval of the thesis:

COUPLED THERMOMECHANICAL ANALYSIS OF CONCRETE HARDENING

submitted by **HALİL İBRAHİM ANDİÇ** in partial fulfillment of the requirements for the degree of **Master of Science in Civil Engineering Department, Middle East Technical University** by,

Prof. Dr. Gülbin Dural Ünver
Dean, Graduate School of **Natural and Applied Sciences** _____

Prof. Dr. Ahmet Cevdet Yalçıner
Head of Department, **Civil Engineering** _____

Assist. Prof. Dr. Serdar Göktepe
Supervisor, **Civil Engineering Department, METU** _____

Prof. Dr. İsmail Özgür Yaman
Co-supervisor, **Civil Engineering Department, METU** _____

Examining Committee Members:

Prof. Dr. Mustafa Tokyay
Civil Engineering Department, METU _____

Assist. Prof. Dr. Serdar Göktepe
Civil Engineering Department, METU _____

Assoc. Prof. Dr. Sinan Turhan Erdoğan
Civil Engineering Department, METU _____

Assoc. Prof. Dr. Afşin Sarıtaş
Civil Engineering Department, METU _____

Assist. Prof. Dr. Ercan Gürses
Aerospace Engineering Department, METU _____

Date: _____

I hereby declare that all information in this document has been obtained and presented in accordance with academic rules and ethical conduct. I also declare that, as required by these rules and conduct, I have fully cited and referenced all material and results that are not original to this work.

Name, Last Name: HALİL İBRAHİM ANDİÇ

Signature   :

ABSTRACT

COUPLED THERMOMECHANICAL ANALYSIS OF CONCRETE
HARDENING

Andiç, Halil İbrahim

M.S., Department of Civil Engineering

Supervisor   : Assist. Prof. Dr. Serdar Göktepe

Co-Supervisor   : Prof. Dr. İsmail Özgür Yaman

February 2015, 72 pages

Thermomechanically coupled modeling of fresh concrete allows us to predict the interaction between thermal and mechanical mechanisms throughout the setting and hardening process. Because of cement hydration, an excessive temperature increase may occur in the interior regions of mass concrete structures. This temperature increase along with the thermal boundary conditions may result in thermal gradients within concrete structures. Owing to the thermal gradients and mechanical constraints, thermally induced stress concentrations may occur. These often manifest themselves in the form of undesired cracks. These cracks eventually deteriorate the concrete unity and shorten the service life of such structures. Although there are several conventional techniques devised to avoid thermal gradients and cracking, they do not always provide an efficient and thorough protection. In this thesis, we propose a thermomechanically coupled finite element model to predict the potential regions of cracking.

To this end, we develop a thermomechanical constitutive model to account for the strong couplings in early-age concrete. The local temperature field in concrete is solved through the transient heat conduction equation where the heat generation due to hydration enters as an internal heat source. The stress concentrations, however, are calculated by solving the balance of linear momentum with a constitutive model that takes into account the dependency of the material parameters on the degree of

hydration and other time-dependent phenomena. We anticipate that the proposed approach can be used to conduct thermomechanically coupled analyses of important mass concrete structures including dams, mass foundations and viaducts to quantify the risk of thermal cracking.

ÖZ

BETON SERTLEŞMESİNİN BAĞLAŞIK TERMOMEKANİK ANALİZİ

Andiç, Halil İbrahim

Yüksek Lisans, İnşaat Mühendisliği Bölümü

Tez Yöneticisi   : Yrd. Doç. Dr. Serdar Göktepe

Ortak Tez Yöneticisi   : Prof. Dr. İsmail Özgür Yaman

Şubat 2015 , 72 sayfa

Taze betonun bağlaşık termomekanik modellenmesi, betonun priz alması ve sertleşmesi sırasındaki termal ve mekanik etkenler arası iletişim hakkında fikir almamızı sağlar. Çimento hidratasyonunun ekzotermik yapısı nedeniyle, masif kütleli yapıların iç kısımlarında yüksek sıcaklık artışı meydana gelebilir. Bu sıcaklık artışı termal sınır koşulları ile birlikte beton içerisinde ısıl gradyanlar meydana getirir. Beton yapının sahip olduğu mekanik kısıtlamalar, ısıl gradyanların beton kütlesinde gerilme yaratmasına neden olur. Bu gerilmeler genellikle istenmeyen çatlaklara yol açar. Çatlak oluşumu betonun bütünlüğünü bozarak, servis ömrünün kısalmasına yol açar. Termal gradyanlardan ve yol açtığı çatlaklardan sakınmanın çeşitli alışılagelmiş yolları olmasına karşın, bu teknikler her zaman etkili koruma sağlayamayabilir. Bu çalışmada, beton yapıda oluşması muhtemel çatlamaları tahmin etmek için sonlu elemanlar metodu ile hesaplanmış bağlaşık termomekanik modeli sunmaktayız.

Bu amaçla, betonun sertleşmesini termomekanik ilk sınır-değer problemi olarak tanımlayarak, bünye denklemleri oluşturulmuştur. Çimento hidratasyonu sonucu ortaya çıkan ısının içsel ısı kaynağı olarak girdiği süreksiz ısı iletim formülü çözülerek yerel sıcaklık değişimleri hesaplanmıştır. Malzeme parametreleri hidratasyon derecesinin ve diğer zamana bağlı olguların fonksiyonu olarak tanımlandı. Sunulan bu yaklaşımın, baraj, masif temel ve viyadük gibi önemli masif beton yapılardaki termal çatlama riskini ölçen bağlaşık termomekanik analizlerde kullanılabileceği umulmak-

tadır.

Anahtar Kelimeler: Taze Beton, Bağlaşık Beton Termomekaniği, Bünye Modellemesi, Sonlu Elemanlar Metodu, ABAQUS

Dedicated Ömer Andiç.

ACKNOWLEDGMENTS

TABLE OF CONTENTS

LIST OF TABLES

TABLES

LIST OF FIGURES

FIGURES

LIST OF ABBREVIATIONS

ACI   American Concrete Institute

ASTM   American Society for Testing and Materials

CAE   Computer-Aided Engineering

CDI   Clasius Duhem Inequality

CPI   Clasius Planck Inequality

CTE   Coefficient of Thermal Expansion

FEM   Finite Element Method

FI   Fourier Inequality

HMT   Hybrid Mixture Theory

OPC   Ordinary Portland Cement

PCC   Portland Cement Concrete

RCC   Roller Compacted Concrete

SHW   State Hydraulic Works

TCAT   Thermodynamically Constrained Averaging Theory

TS   Turkish Standards

UMAT   User Material Subroutine

UMATHT   User Material Thermal Subroutine

XPS   Extruded Polystrene

CHAPTER 1

INTRODUCTION

Concrete has been used as a civilization material for thousands of years. With the rising needs of humanity, properties and geometry of concrete have developed and the intended use of it has spread to different areas. Today, concrete is preferred for the construction of buildings, bridges, viaducts, dams, drinking water utilities, roads, tunnels etc. By volume, the largest manufactured product in the world today is concrete.

The reason behind becoming the most manufactured product, at least three main advantages can be said. First, Portland Cement Concrete (PCC) has an advanced resistance to water. In the ancient times, water transporting and storing could be handled with concrete aqueducts and waterproof concrete stores. Today, the necessity of electric power makes humanity build bigger concrete dams. The other characteristic property of PCC is the ease of forming it into desired structural element shape. The plastic behavior of concrete provides an advantage and this plastic form longs for hours. Besides, raw materials of PCC can be found in the nature easily and they are relatively inexpensive. The term concrete will refer to PCC in this thesis.

These advantages make concrete more popular and therefore, the consumption rate of concrete keeps the positive trend. With more needs of civilization, the bigger sized concrete elements have begun to use. Concrete dams, viaducts, foundations and these kinds of bigger sized structures are called mass concrete. The development of new concrete technologies and increasing the necessity of concrete consumption brings new and big challenges with them. Especially in mass concrete structures, because of the volume and the plain structure of concrete, vital problems may occur. During

the construction of mass concrete structures, cement hydration, which is an exothermic reaction, causes an excessive temperature increase in the concrete body. Owing to mechanical restraints and thermal boundary conditions, thermal cracks may occur on concrete surface. This phenomenon is studied within the framework of coupled chemo-thermo-mechanics. To understand the behavior of the world's most commonly used construction material and simulate the concrete hardening, a mathematical model is required.

In this thesis, it is aimed to develop a mathematical model to simulate the hydration progress at a macro-scale and its effect on the macroscopic properties of hardening concrete in the early-age. To this end, the three-dimensional coupled problem of concrete chemo-thermo-mechanics by using the proposed model is solved and the potential of the model in simulating the behavior of concrete for temperature evolution, stress development, and thermal cracking estimation are conducted.

1.1 Concrete

Concrete is a composite material that includes ordinary portland cement (OPC), water and aggregate in its simple form. Additional chemical or mineral admixtures can be added in concrete mixture when needed. A detailed description of concrete is made by American Society for Testing and Materials (ASTM): "*Concrete is a composite material that consists essentially of a binding medium within which are embedded particles or fragments of aggregate. In hydraulic-cement concrete, the binder is formed from a mixture of hydraulic cement and water*" [11].

The product of the reaction of cement with water is called cement paste. In the early ages of concrete hardening, cement paste get into a plastic form. However, once the setting takes place, cement paste gains rigidity and concrete becomes hardened. The main reason of this phase change is chemical reactions of hydration. A typical mesostructure of concrete containing aggregate and cement paste in demonstrated in Figure 1.1.

In order to understand the thermomechanics of concrete better, the properties of aggregates and portland cement are discussed in Sections 1.1.1 and 1.1.2, respectively.

2
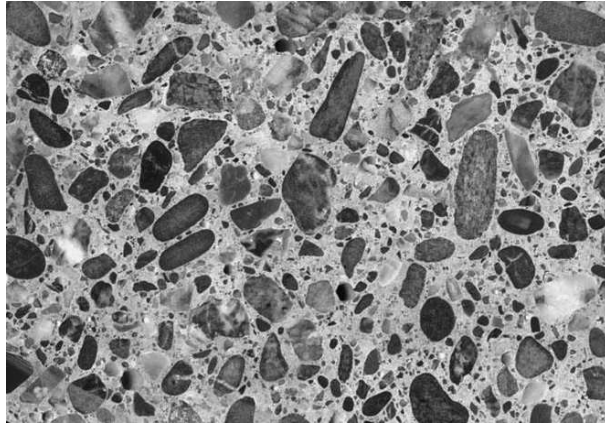
Figure 1.1: Two fundamental phases constituting the concrete mesostructure: aggregate particles of various shapes and sizes and the cement paste as a binding medium [52].

1.1.1 Properties of Aggregates

Aggregates are natural or artificial granular materials. They constitute about 75% of the concrete volume. Natural aggregates are mostly obtained from sand, gravel, and crushed rock and they are often used in the mixture of normal strength concrete. The size, shape and texture of aggregate has an important effect on the concrete quality. According to Turkish Standard TS 706 [63], aggregates that pass the sieve with a 4 mm square opening, are called fine aggregates. The retained aggregates on the same sieve are classified as coarse aggregates. Both aggregate types have different characteristics on the behavior of concrete. Coarse aggregate provides volumetric stability and constitutes the rigidity of concrete. In Figure 1.2, the representative stress-strain curves of aggregate, concrete, and cement paste are depicted.

Aggregate is the cheapest raw material of concrete. It fills a large volume in concrete member and reduces the cost by replacing cement. Through its high performance on compressive strength, coarse aggregates provide an important contribution to concrete's strength. In addition, fine aggregates fill the undesired voids and makes concrete more workable and imporous.

Other material parameters are also afffected by aggregates. According to Kodur [43], the specific heat capacity and the thermal expansion coefficient of concrete may vary
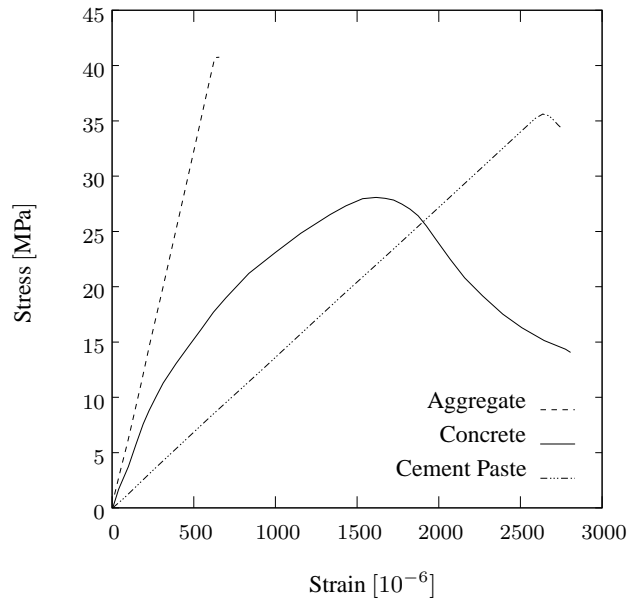
Figure 1.2: Stress-strain curves of aggregate, concrete and hydrated cement paste at the same loading rate [47].

with the aggregate type. Moreover, the placement temperature of concrete structures are highly influenced by the temperature of aggregate. Malkawi, Mutasher and Qui [50] performed a study on placing temperature of roller compacted concrete (RCC) and the predicted the contribution of aggregates to the placing temperature. Their study shows that the initial temperature of concrete is highly influenced by the temperature of aggregates.

1.1.2 Portland Cement

Portland cement is composed of limestone and clay and is defined as a hydraulic binder. Heating the raw materials of cement at 1450 °C in a rotary kiln, the clinker is produced. The clinker is mixed with a certain amount of gypsum to make Portland cement. Cement is the main binding material of concrete structures. It can be blended with admixtures to change the characteristics of concrete. In mass concrete structures, mineral admixtures are preferred to strengthen the microstructure of concrete. Addition of mineral admixtures like fly ash or silica fume fills the undesired voids in the microstructure of cement paste and decreases the porosity of concrete section.

The plasticity of cement paste improves the workability of concrete when the ingredients of concrete are mixed until the setting. The primarily function of cement paste in concrete is to accomplish a coherence with aggregates and reduce the voids near aggregate particles by covering their surfaces. By the help of cement paste plasticity in the early ages of concrete, concrete becomes workable when the materials are mixed until the setting occurs. Therefore, this property of cement paste allows for the achievement of rigid concrete in a desired shape and size.

Clinker has four major compounds. These are tricalcium silicate (C_3S), dicalcium silicate (C_2S), tricalcium aluminate (C_3A) and tetracalcium alumino ferrite (C_4AF). The characteristics of these compounds are different. Since clinker and a limited amount of gypsum constitute cement, the major compounds of clinker can be assumed as the major compounds of cement [28, 55].

1.2 Cement Hydration Kinetics

Cement hydration is a complex chemophysical process. The compounds of cement have different characteristics and independent effects on the cement hydration.

The degree of each compound's behavior in the rate of hydration, the amount of liberated heat, and their contribution to strength of early-age concrete are qualitatively given in Table 1.1.

Table 1.1: Relative behavior of major compounds of cement [27]

	C_3S	C_2S	C_3A	C_4AF
Hydration rate	Moderate	Slow	Fast	Moderate
Heat liberation	High	Low	Very High	Moderate
Contribution to strength	High	Low	Low	Low

The contribution of C_3A to the strength of early-age concrete is high for the first couple of hours of hydration. However, this contribution remains same for the rest of hydration and its qualitative degree is indicated as low in the Table 1.1. Contributions of cement compounds to concrete strength for 100 hours are depicted in Figure 1.3.
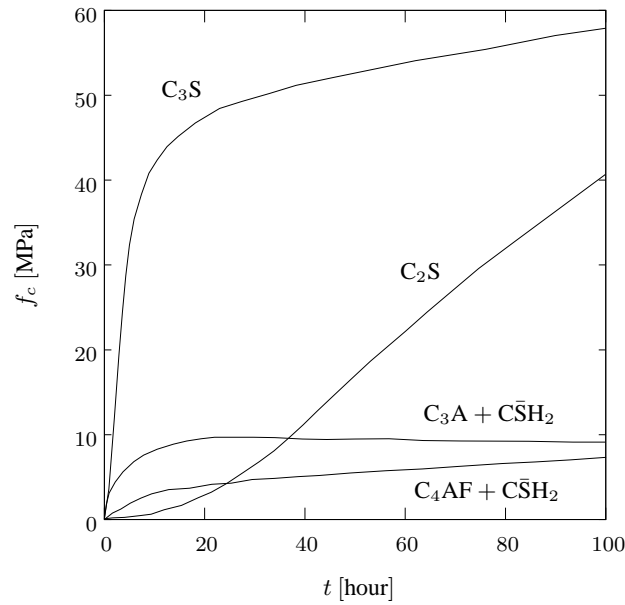
Figure 1.3: Contribution of cement compounds to the strength of early-age concrete [53].

Hydration of major compounds are independent from each other. Therefore, hydration mechanisms of compounds are evaluated seperately as hydration of silicates and aluminates.

1.2.1 Hydration of the Silicates

The reaction of C_3S and C_2S with water produces the same two products.

$$2\,C_3S + 4\,H \longrightarrow C_3S_2H_3 + 3\,CH \tag{1.1}$$

$$2\,C_2S + 6\,H \longrightarrow C_3S_2H_3 + CH \tag{1.2}$$
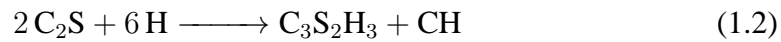
The first product $C_3S_2H_3$ is calcium silicate hydrate gel and it is called C-S-H gel. The other product is calcium hydroxide (CH). According to Table 1.1 and Figure 1.3, C_3S and C_2S are responsible of early-age concrete strength gaining. Also, CH does not have a significant contribution to the concrete strength. Therefore, C-S-H gel is accepted as the main source of the early-age concrete's strength gain.

6

1.2.2 Hydration of the Aluminates

C_3A is a very reactive product. Its hydration is very immediate and liberates large amount of heat. Because of its rapid reaction, cement gains an immediate stiffening and this event is known as flash set. The reason for blending gypsum ($C\bar{S}H_2$) with clinker during the cement production is to avoid flash set. The hydration of C_3A with gypsum produces two products.

$$C_3A + C\bar{S}H_2 + 10H \longrightarrow C_4A\bar{S}H_{12} \tag{1.3}$$

$$C_3A + 3C\bar{S}H_2 + 26H \longrightarrow C_6A\bar{S}_3H_{32} \tag{1.4}$$

The first product is the calcium-alumino-monosulfohydrate, which is known as AFm. AFm is not stable and it may react with more gypsum and causes to produce $C_6A\bar{S}_3H_{32}$.

$$C_4A\bar{S}H_{12} + 2C\bar{S}H_2 + 16H \longrightarrow C_6A\bar{S}_3H_{32} \tag{1.5}$$
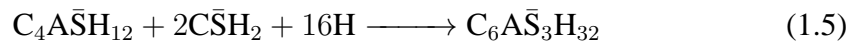
$C_6A\bar{S}_3H_{32}$ is the calcium-alumino-trisulfohydrate, which is also known as ettringite. Ettringite is a hazardous product for concrete. If ettringite forms, an expansion occurs in the cement paste and it creates a serious durability issues in hardened concrete. In the lack of gypsum in the cement, flash setting occurs. If a high amount of gypsum enters the reactions, this may result in expansion and cracking.

The hydration of C_4AF is very similar to the hydration of C_3A. C_4AF requires gypsum to form and it causes expansion and heat liberation. This formation is slower and liberates less heat than the formation of C_3A.

1.2.3 Heat Liberation

The hydration of cement compounds is an exothermic reaction. During these reactions, heat is liberated. This is called the heat of hydration. The heat of cement hydration has different influences in concrete technology. The comparatively low thermal conductivity of concrete causes a rise in temperature in the interior of giant mass concrete structures. Simultaneously, the exterior parts of the structure lose heat, and therefore, temperature gradients occur. With the mechanical restraints, this gradient may result in serious cracking. On the other hand, the liberated heat during hydration of cement may prevent water freezing in the capillary pores in cold weather.

The relative contributions of cement compounds to the heat liberation of hydration are given in Table 1.1. Their overall effect on the curve of heat liberation rate is depicted in Figure 1.4. The cumulative liberated heat obtained by integrating the rate of heat liberation over time (Figure 1.4) is demonstrated in Figure 1.5.
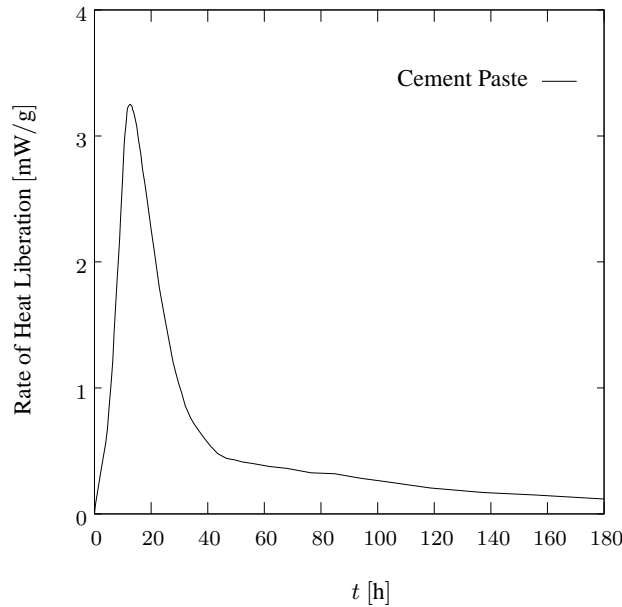
Figure 1.4: A typical heat liberation rate of a cement paste during the early hardening period under isothermal conditions [34].

For further information on heat liberation during hydration, the reader is referred to [34, 56, 22].

1.2.4   Effect of Mineral Admixtures on Heat Liberation

Replacing cement content with mineral admixtures in concrete mixture has several advantages. Using mineral admixtures gives an opportunity of reducing the temperature increase of concrete nearly in direct proportion to the replaced cement amount. The total heat of hydration liberated by the mineral admixtures is almost half of the average heat produced by the cement hydration [52].

The most commonly used mineral admixtures for the construction of mass concrete structures are fly ash and silica fume. Replacement of portland cement by fly ash in mass concrete structures has been performed since the 1930s. Fly ash has a lower

8
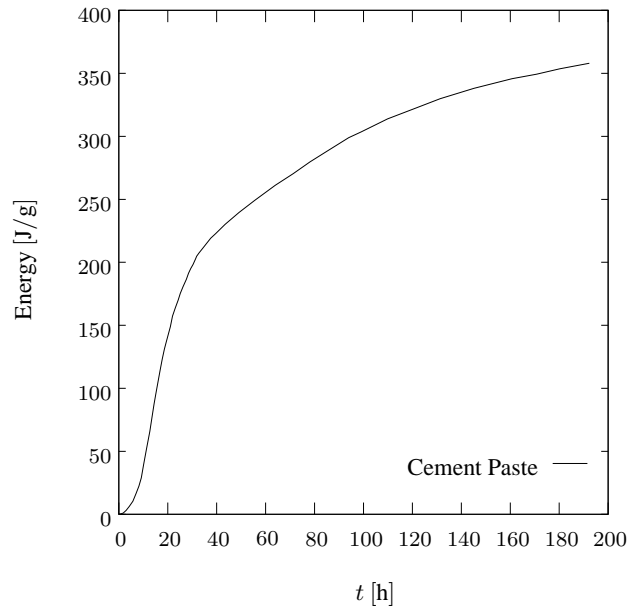
Figure 1.5: Liberated heat of hydration of cement paste measured by isothermal calorimetry [34].

rate of heat liberation than the portland cement. Besides, heat of hydration of concrete which includes 10% silica fume is higher than the concrete with no additives in the first 72 hours. However, silica fume added concrete liberates approximately 8% - 10% less heat in total [28]. This condition can be observed in Figure 1.6. In the literature, there are several studies about the effect of mineral admixtures on heat liberation. For further information, the reader is referred to [60, 34, 44].

1.3 Mass Concrete

Concrete has numerous areas of usage and each concrete structure has different ambient and conditions. For the construction of structures with large dimensions as concrete gravity dams, mass foundations, viaducts etc., massive concrete blocks are required. These kinds of structures are called mass concrete. American Concrete Institute (ACI) [10] defines mass concrete as: *"any volume of concrete with dimensions large enough to require that measures be taken to cope with generation of heat from hydration of the cement and attendant volume change, to minimize cracking"*. In Figure 1.7, examples of different types of mass concrete structures are placed.

9
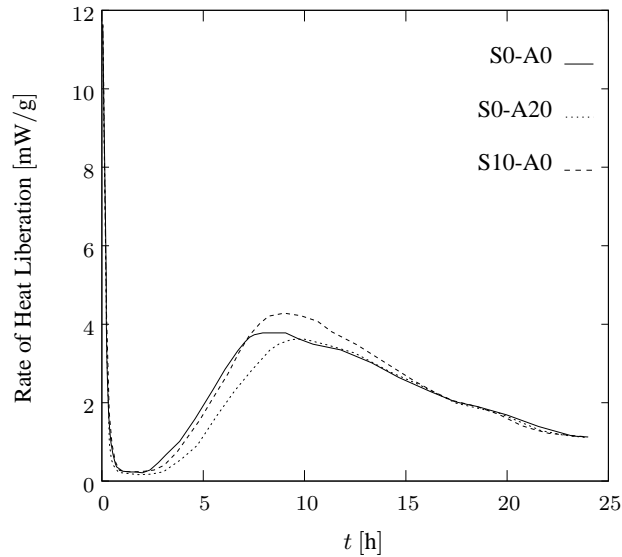
Figure 1.6: Heat liberation rate of cement, silica fume and fly ash mixtures with 0.50 water-cement ratio under isothermal conditions. The letter 'S' and 'A' represents the silica fume and fly ash, respectively and the numbers are the percentage of additives in the mixture by weight [44].

Casting of large volumes of unreinforced (plain) concrete for mass concrete structures may cause thermal cracking because of the three reasons: low thermal conductivity of concrete, the heat of hydration of cement and the external mechanical restraints. As a result of hydration reaction, liberated heat of hydration causes an increase in temperature in the interior of structure and because of the comparatively low thermal conductivity of concrete, heat can not be conducted with ambient easily. As a result of these circumstances, temperature gradient occurs and because of external mechanical restraints, thermal cracking may appear [54].

In order to prevent thermal cracking in mass concrete structures, the effects of the hydration can be limited in three conventional methods:

- Selection of proper material composition to reduce the heat liberation rate during hydration.
- Controlling the concrete block geometry and the time interval between block casting to allow heat dissipation.
- Controlling the placing temperature of concrete or using post-cooling techniques to reduce the thermal gradient.

10
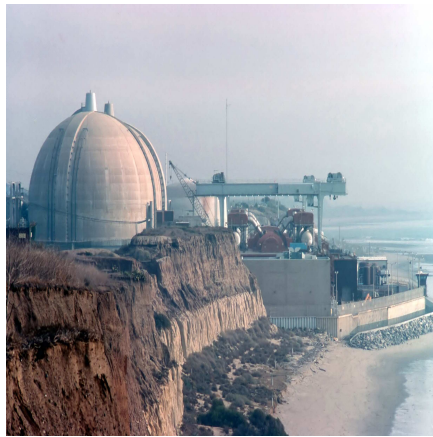
Figure 1.7: Examples of mass concrete structures. a) Deriner Dam from Turkey [2], b) mass foundation from United States of America [3], c) nuclear power plant from United Arab Emirates [4], and d) offshore platform from Norway [6].

Generally, using low heat cement, which has low amount of C_3S, is beneficial for decreasing the temperature. In Figure 1.8, adiabatic temperature rise in mass concretes with different types of cement is depicted [47]. In addition to cement replacement, adding mineral admixture, especially fly ash, is also an effective way of reducing temperature value. As indicated in Section 1.2.4, the total heat of hydration liberated by fly ash is lower than the portland cement (see Figure 1.6). Besides, placing temperature of concrete is highly influenced by the initial temperature of aggregates [50].

Mass concrete structures involve enormous volumes of concrete and casting is per-
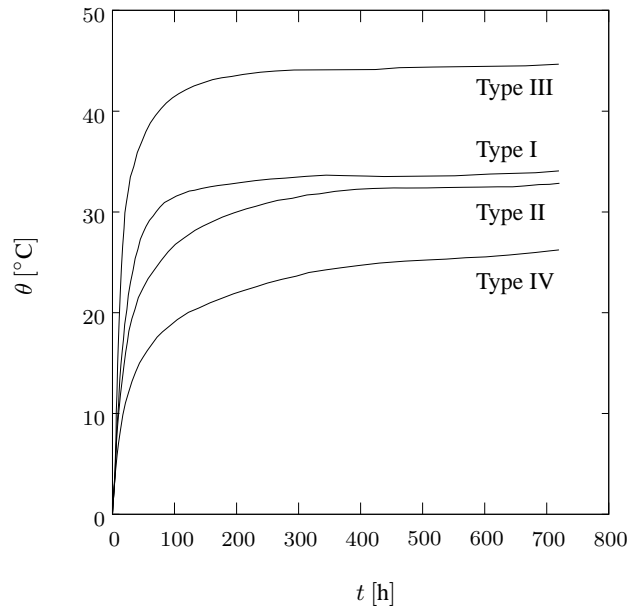
Figure 1.8: Adiabatic temperature rise in mass concretes with different types of cement [47]. Four types of cement, which are classified by ASTM C150, are compared [12]. Type I, Type II, Type III and Type IV cements are used for general use, moderate heat of hydration, high early strength, and low heat of hydration, respectively.

formed with comparatively smaller blocks. Geometry and casting time interval of concrete blocks have an influence on the heat dissipation and the evolution of temperature of concrete. To determine the optimum values of these parameters, Fairbairn et al. [29] conducted an optimization study using genetic algorithms. They studied on the construction cost, effect of material types, placing temperature, the height of blocks and the time interval between blocks. According to their study, for the minimum cost, the optimum values of placing temperature, height of block and casting frequency are determined as 19 C$^\circ$, 1.25 m and 5 days, respectively. Also, as reported by Bureau of Indian Standards [9], the placing frequency must be minimum 3 days. Moreover, during the construction of Hoover Dam, the time delay between the block castings is applied as 3 days and the block height is limited to 1.5 m [25].

There are several methods that decrease the temperature gradient of the concrete structure. These methods are generally divided into 2 category: pre-cooling and past-cooling. Pre-cooling methods reduce the initial temperature of mixing materials of concrete. A typical example of this category is using ice instead of water into con-

crete. Also, controlling the intial temperature of aggregates decreases the placing temperature of concrete. In the other hand, post-cooling methods are applied after casting. Pipe cooling method is applied in numerous works of mass concrete through its effectiveness in reducing the interior temperature. In this technique, pipes are embedded before casting and after concrete placement, flow of cool water prevents the internal temperature rise. However, cool water inside the pipe creates a greate temperature drop close to the cooling pipes and this very low temperature degree produces a temperature gradient within the concrete, which induce great tensile stresses [48]. Furthermore, covering the external surface of concrete with an insulator maintains the external temperature of concrete and decreases the temperature difference. In addition to these conventional techniques, Ha, Jung and Cho [35] presents a novel method to control the thermal cracking in mass concrete structures. They developed an automated curing system that avoids the temperature gradient between the internal and external surfaces of the structure.

Despite the preventing techniques, mass concrete structures have thermal cracking risk and the possible cracking may results with serious hazards. To understand the behavior and predict the cracking potential of concrete structures, a three-dimensional constitutive model is required. The model must be able to calculate the evolutions of temperature and stress and also consider the couplings between the chemical, thermal and mechanical fields. By the help of this model, the tensile strength and the maximum principle stress of concrete can be calculated and the possible cracking regions may be predicted. Cervera, Oliver and Prato [18] developed a numerical procedure for the simulation of the construction process of RCC dams. Moreover, Kim, Kim and Yang [40] performed a thermal analysis of mass concrete structures with pipe-cooling system. They modeled pipe-cooling system inside the structure and simulated the evolution of temperature.

1.4   Modeling of Concrete at Early-Ages

The complex mechanism of cement hydration is briefly introduced in Section 1.2. Chemical reactions of hydration, concrete setting, heat liberation and change of mechanical material parameters of concrete constitute a complicated coupled problem.

13

The modeling studies of these coupled effects within Continuum Thermomechanics began in the last two decades [17, 65, 66, 67].

1.4.1 Reactive Porous Media

The chemo-thermo-mechanical model used in this thesis is mainly based on the theory of reactive porous media, which is introduced by Coussy [20], and application of this theory to concrete developed by Ulm and Coussy [65, 66]. In the concrete application of the theory, the hydration reaction of concrete is viewed from the macroscopic scale. The solid part of concrete is formed of unhydrated cement and hydrates. During the hydration reaction, water diffuses from the layers of already formed hydrates to the unhydrated cement particles. When the water meets with the unhydrated parts, new hydrates occurs and the water is combined. Thus, the diffusion of water over the layers of already formed hydrates can be considered as the dominant process of the hydration [67].

In the Theory of Reactive Porous Media, a closed chemical system is assumed and the chemical reactions are modeled with the help of local internal variables. Because of the different reactivity of hydration products, chemical system is simplified and the hydration process is modeled as simplified cement hydration. Temperature and the degree of hydration are assumed as the two essential variables of this closed thermomechanical model and the free energy is formulated in terms of these variables. The evolution of the degree of hydration is determined by an Arrhenius-type ordinary differential equation. The liberated heat during the chemical reactions enters the equation of temperature evolution as a heat source. The time evolution of mechanical properties of concrete during hydration is called aging. This phenomenon is modeled with the concept of degree of aging. The material parameters of these models are determined with the help of different experimental results, local simulations are performed at material point.

1.4.2 Multiphase Porous Media

The chemically closed studies neglect the mass transfer inside concrete. Recently, these studies have been started to improve with considering the mass transfer with ambient (hygro effects) by researchers. Gawin, Pesavento and Schrefler [31, 32, 58] published several articles about the hygro-thermo-chemo-mechanical modelling of concrete at early ages. In these articles, concrete is considered as a multiphase porous viscoelastic material, which is in solid, liquid and gaseous forms. This modeling approach is called Multiphase Porous Media.

In Multiphase Porous Media, in addition to conservation of linear momentum (mechanical balance) and conservation of energy (thermal balance), different conservation of mass equations, which consider the diffusion inside the concrete and mass transfer with ambient, are used. This very complex approach requires a large number of material parameters and variables. The difficulty in the determination of the material parameters makes this model more unrealistic for applying in the analysis of boundary-value problems. Because of the difficulties on modeling progress, there are very few numerical simulation studies on Multiphase Porous Media and these studies are mostly limited in two dimensional space. For these studies, the reader is referred to Jendele, Šmilauer and Červenka [37] and Valentini and et al. [68].

In the theory of multiphase porous media, concrete is evaluated as a multiphase porous visco-elastic material. In the media, chemical reactions, phase changes, and aging of material properties are taken into account. This approach is based on the hybrid mixture theory (HMT) developed by Hassanizadeh and Gray [36]. HMT considers a multiscale (microscale, mesoscale and macroscale) problem involving shrinkage/swelling media. The concrete structure is considered to be formed by more than one phase, which are oftenly liquid and solid [14]. Balance equations are introduced at the microscale level and then averaged by HMT to obtain the macroscopic balance equation. However, constitutive laws are directly defined at macroscopic level.

1.4.3 Thermodynamically Constrained Averaging Theory

Modeling of porous media should be multiphase and must consider the different scales. These are the main aspects of the Thermodynamically Constrained Averaging Theory (TCAT) developed by Gray and Miller in 2005 [33]. The procedure of the TCAT is very similar to the HMT. Balance equations are first defined at the microscale and they are upscaled by averaging theorems to introduce the macroscopic balance equations. The principal difference between the TCAT and the HMT is that in the HMT the entropy inequality is assured only at the macroscale and in the TCAT, balance equations for entropy are written at the microscale for each phase, and then upscaled. There are very few application study of this theory in the literature. By using this theory, Sciume [61] presented a thermo-hygro-chemo-mechanical early-age concrete model and extended this model to tumor growth.

1.5 Aim of Thesis

The aim of this thesis is to model the coupled thermomechanical behavior of the concrete hardening by developing a three-dimensional constitutive model. To account for the cross coupling between chemical, thermal, and mechanical effects, the theoretical formulation of the problems is carried out within the framework of continuum thermodynamics for closed systems. In particular, the Theory of Reactive Porous Media is followed. Since it is also aimed to conduct predictive numerical simulations of realistic coupled initial boundary-value problems, the developed theoretical model along with its algorithmic formulation is implemented into a commercial finite element tool as a user material model. The model parameters are then identified by fitting the model response to the experimental data taken from the literature. By using the identified material parameters in the computer implementation, the predictive numerical analyses of different concrete structures are performed. These analyses do not only cover the uneven temperature field evolution but also the development of stress concentrations in mass concrete structures. In this thesis, principles of porous media mechanics are followed. Appropriate material parameters for the developed model are determined and application of the theory to the dam example is conducted.

1.6 Scope and Outline

In **Chapter 1**, the basic definition of the terms used in the thesis is given. Previous works carried on the cement hydration and early-age concrete modeling are introduced.

Chapter 2 is devoted to the fundamentals of continuum thermomechanics. The kinematics and state variables are given. Balance laws are introduced in their global and local forms. Two fundamental differential equations, namely the balance of linear momentum and the transient heat conduction equations are derived. Besides, dissipation is introduced.

In **Chapter 3**, the three-dimensional continuous formulation of the coupled initial boundary-value problem of early-age thermomechanics is introduced. In this contribution, essential governing differential equations of the problem are derived. Constitutive and aging equations are introduced. Additionally, special forms of thermal and mechanical material parameters are stated.

Chapter 4 deals with the potential of proposed constitutive model with three representative numerical problems. The first example problem is concerned with the local simulation of the results in Bentz, Waller and Larrard [15]. In this study, simulation of temperature, chemical affinity and compressive strength evolutions are presented. In the second example, experiments, which are conducted for Ilısu Dam are simulated qualitatively. For the last example, Deriner Dam is modeled and stress distribution of the structure is computed. Besides, the crack estimation study for the Deriner Dam is also performed.

This thesis is concluded with a summary, some remarks, and outlook in **Chapter 5**.

CHAPTER 2

THERMOMECHANICS OF THE THREE-DIMENSIONAL CONTINUUM

This chapter is devoted to the fundamental formulations of geometrically linear continuum mechanics and the key equations of thermodynamics that govern the thermomechanical behavior of materials. In Section 2.1, kinematics at small strains and the external state variables are introduced. Furthermore, the descriptions of the strain tensor and the temperature field, which are the external state variables of thermomechanics, are given. In Section 2.2, the stress tensor and the heat flux are introduced along with their relations with the stress traction vector and the heat flux vector through the Cauchy's theorem. In Section 2.3, conservation laws for several physical phenomena are introduced as balance laws and their global and local forms are derived. With these conservation laws, two fundamental governing differential equations of thermomechanics are introduced by accounting for their mutual coupling. In Section 2.4, the concept of dissipation according to the second law of thermodynamics is introduced.

2.1 Kinematics and State Variables

In continuum mechanics, a substance, which may exist in a solid, liquid, or gaseous state, can be considered as a material body. Before introducing the essential equations of thermomechanics, the motion of a deformable solid body is described. To this end, let us assume the configuration of our material body within the Euclidean space is denoted by $\mathcal{B} \subset \mathbb{R}^3$ at time $t \in \mathbb{R}_+$. $\boldsymbol{u}(\boldsymbol{x}, t)$ is the displacement map describing the displacement field of a material point $\mathcal{P}$ located at $\boldsymbol{x} \in \mathcal{B}$ at time $t \in \mathcal{I}$. This mapping

can be defined as,

$$\boldsymbol{u}(\boldsymbol{x},t) : \begin{cases} \mathcal{B} \times \mathcal{I} & \to \mathbb{R}^3 \,, \\ (\boldsymbol{x},t) & \to \boldsymbol{u}(\boldsymbol{x},t) \,. \end{cases} \tag{2.1}$$

The time rate of the deformation field gives the velocity

$$\boldsymbol{v}(\boldsymbol{x},t) := \frac{\partial \boldsymbol{u}(\boldsymbol{x},t)}{\partial t} = \dot{\boldsymbol{u}}(\boldsymbol{x},t) \,, \tag{2.2}$$

and the rate of velocity gives the acceleration field

$$\boldsymbol{a}(\boldsymbol{x},t) := \frac{\partial \boldsymbol{u}(\boldsymbol{x},t)}{\partial t} = \dot{\boldsymbol{v}}(\boldsymbol{x},t) = \ddot{\boldsymbol{u}}(\boldsymbol{x},t) \,. \tag{2.3}$$

The strain tensor at $\boldsymbol{x} \in \mathcal{B}$ is defined by

$$\boldsymbol{\varepsilon}(\boldsymbol{x},t) := \operatorname{sym}(\nabla \boldsymbol{u}) := \frac{1}{2}(\nabla \boldsymbol{u} + \nabla^T \boldsymbol{u}) \,. \tag{2.4}$$

The temperature field $\theta(\boldsymbol{x},t)$ and the displacement field $\boldsymbol{u}(\boldsymbol{x},t)$ constitute the external state variables of thermomechanics. Both variables depend on the position and time.

$$\operatorname{State}(\boldsymbol{x},t) = \{\boldsymbol{u}(\boldsymbol{x},t), \theta(\boldsymbol{x},t)\} \tag{2.5}$$

2.2 Stress Tensor and Heat Flux

Let $\mathcal{P} \subset \mathcal{B}$ denote an arbitrary part of a body $\mathcal{B}$. The part $\mathcal{P}$ has an interaction with the rest part of the body, and this thermomechanical interaction is represented by two elemental quantities of continuum mechanics: the stress traction vector $\boldsymbol{t}$ and the outward heat flux h. Both quantities are linearly dependent on the orientation of the cut $\mathcal{P}$ at $\boldsymbol{x} \in \partial\mathcal{P}$ and characterized by the surface unit normal $\boldsymbol{n}$. The stress traction vector $\boldsymbol{t}$ and the heat flux h can be related to the stress tensor $\boldsymbol{\sigma}$ and the heat flux vector $\boldsymbol{q}$ through the Cauchy's theorem.

$$t = \boldsymbol{\sigma}\,\boldsymbol{n} \quad \text{and} \quad h = \boldsymbol{q} \cdot \boldsymbol{n} \,. \tag{2.6}$$

The representation of the stress tensor and heat flux is given in Figure 2.1.

20
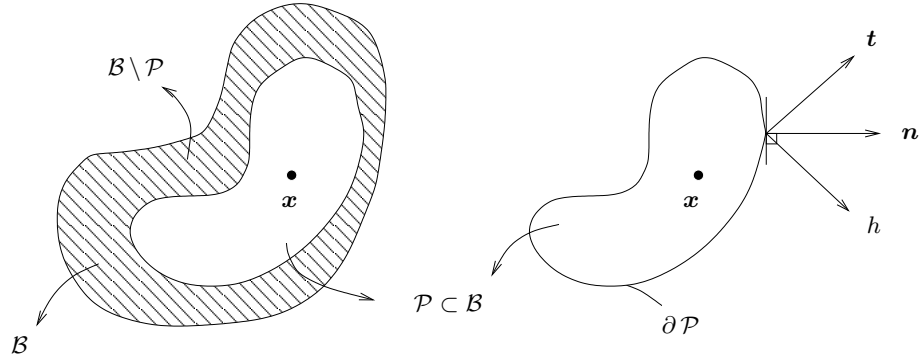
Figure 2.1: Representation of stress tensor t and heat flux h of a part $\mathcal{P} \subset \mathcal{B}$ with a boundary of $\partial\mathcal{P}$

2.3 Fundamental Conservation Laws

In this section, the balance laws for the part $\mathcal{P} \subset \mathcal{B}$ are formulated. We first define the physical fields of thermomechanics.

$$
\begin{aligned}
&\text{(i)} \quad \text{Mass} && m := \int_{\mathcal{P}} \rho \, dV \\[2mm]
&\text{(ii)} \quad \text{Linear Momentum} && \mathbf{I} := \int_{\mathcal{P}} \rho \, \boldsymbol{v} \, dV \\[2mm]
&\text{(iii)} \quad \text{Angular Momentum} && \boldsymbol{\mathcal{D}}_0 := \int_{\mathcal{P}} \boldsymbol{x} \times \rho \, \boldsymbol{v} \, dV \\[2mm]
&\text{(iv)} \quad \text{Kinetic Energy} && \mathcal{K} := \int_{\mathcal{P}} \frac{1}{2} \rho \, \boldsymbol{v} \cdot \boldsymbol{v} \, dV \\[2mm]
&\text{(v)} \quad \text{Internal Energy} && \mathcal{E} := \int_{\mathcal{P}} \rho \, e \, dV \\[2mm]
&\text{(vi)} \quad \text{Entropy} && \mathcal{H} := \int_{\mathcal{P}} \rho \, \eta \, dV \\[2mm]
&\text{(vii)} \quad \text{Entropy Production} && \Gamma := \int_{\mathcal{P}} \rho \, \gamma \, dV
\end{aligned}
\tag{2.7}
$$

where the fields $\rho(\boldsymbol{x},t)$, $\boldsymbol{u}(\boldsymbol{x},t)$, $\boldsymbol{v}(\boldsymbol{x},t)$, $e(\boldsymbol{x},t)$, $\eta(\boldsymbol{x},t)$, $\gamma(\boldsymbol{x},t)$ describe the mass density, displacement, velocity, internal energy, entropy, and entropy production rate, respectively. The terms e, η, and γ are defined per unit mass.

The volume loads, which are the body forces $\boldsymbol{b}$ and the heat source r, and the surface loads, which include the stress traction vector $\boldsymbol{t}$ and the heat flux vector $\boldsymbol{q}$, act on the

21

part $\mathcal{P} \subset \mathcal{B}$ and on its surface $\partial \mathcal{P}$, respectively. The heat source is defined per unit mass. Global quantities associated with the volume and surface loads are defined as

$$
\begin{aligned}
\text{(i)} \quad &\text{Mechanical Force} & \boldsymbol{\mathcal{F}} &:= \int_{\mathcal{P}} \rho \, \boldsymbol{b} \, dV + \int_{\partial \mathcal{P}} \boldsymbol{t} \, dA \\
\text{(ii)} \quad &\text{Mechanical Couple} & \mathbf{M}_0 &:= \int_{\mathcal{P}} \boldsymbol{x} \times \rho \, \boldsymbol{b} \, dV + \int_{\partial \mathcal{P}} \boldsymbol{x} \times \boldsymbol{t} \, dA \\
\text{(iii)} \quad &\text{Mechanical Power} & \mathcal{P} &:= \int_{\mathcal{P}} \rho \, \boldsymbol{b} \cdot \boldsymbol{v} \, dV + \int_{\partial \mathcal{P}} \boldsymbol{t} \cdot \boldsymbol{v} \, dA \qquad (2.8) \\
\text{(iv)} \quad &\text{Thermal Power} & \mathcal{Q} &:= \int_{\mathcal{P}} \rho \, r \, dV - \int_{\partial \mathcal{P}} h \, dA \\
\text{(v)} \quad &\text{Entropy Power} & \mathcal{S} &:= \int_{\mathcal{P}} \rho \, \frac{r}{\theta} \, dV - \int_{\partial \mathcal{P}} \frac{h}{\theta} \, dA
\end{aligned}
$$

These quantities have both volume and surface integral terms.

2.3.1 Global Forms

The relationships between the physical fields (2.7) and the thermodynamic sources (2.8) are described by the fundamental balance laws of continuum mechanics. These relationships are written in the following global forms.

$$
\begin{aligned}
\text{(i)} \quad &\text{Conservation of Mass} & \frac{d}{dt}[m] &= 0 \\
\\
\text{(ii)} \quad &\text{Conservation of Linear Momentum} & \frac{d}{dt}\mathbf{I} &= \boldsymbol{\mathcal{F}} \\
\\
\text{(iii)} \quad &\text{Conservation of Angular Momentum} & \frac{d}{dt}\mathbf{D}_0 &= \mathbf{M}_0 \qquad (2.9) \\
\\
\text{(iv)} \quad &\text{Conservation of Energy} & \frac{d}{dt}[\mathcal{K} + \mathcal{E}] &= \mathcal{P} + \mathcal{Q} \\
\\
\text{(v)} \quad &\text{Conservation of Entropy} & \Gamma := \frac{d}{dt}[\mathcal{H}] - \mathcal{S} &\geq 0
\end{aligned}
$$

The conservation of mass, which is also known as the continuity equation, represents the mass equilibrium in a closed system. The conservation of energy and entropy are the first and second laws of thermodynamics, respectively. For the volume of $\mathcal{P} \subset \mathcal{B}$, these conservation equations are expressed as global statements as in (2.9).

2.3.2 Local Forms

In order to obtain the local differential forms of the global conservation equations expressed in integral forms in (2.9), the following steps are followed.

- **Step 1:** Insert the Cauchy's Theorem

$$t = \sigma n \qquad \text{and} \qquad h = q \cdot n \tag{2.10}$$

- **Step 2:** Transform the surface integrals into volume integrals by the Gauss-Integral theorem.

$$\int_{\partial \mathcal{P}} (\cdot) \cdot n \, dA = \int_{\mathcal{P}} \text{div}(\cdot) \, dV \tag{2.11}$$

- **Step 3:** Apply the localization theorem.

$$\lim_{\mathcal{P} \to dV} \int_{\mathcal{P}} (\cdot) \, dV = 0 \qquad \Longleftrightarrow \qquad (\cdot) = 0 \tag{2.12}$$

Conservation of Mass

Substituting $(2.7)_1$ into $(2.9)_1$, we obtain

$$\frac{d}{dt}[m] = \frac{d}{dt} \int_{\mathcal{P}} \rho \, dV = \int_{\mathcal{P}} \frac{d\rho}{dt} \, dV = \int_{\mathcal{P}} \dot{\rho} \, dV = 0 \, . \tag{2.13}$$

Through the localization theorem, we end up with

$$\lim_{\mathcal{P} \to dV} \int_{\mathcal{P}} \dot{\rho} \, dV = 0 \Longleftrightarrow \dot{\rho} = 0 \tag{2.14}$$

This final equilibrium indicates that the mass density of a body is constant for closed systems within the geometrically linear theory.

Conservation of Linear Momentum

Insertion of $(2.7)_2$ into $(2.9)_2$ with $(2.8)_1$ leads us to

$$\frac{d}{dt} \int_{\mathcal{P}} \rho \, v \, dV = \int_{\mathcal{P}} (\dot{\rho} \, v + \rho \, \dot{v}) dV = \int_{\mathcal{P}} \rho \, b \, dV + \int_{\partial \mathcal{P}} t \, dA \, . \tag{2.15}$$

where $\dot{\rho} \, v = 0$ as explained in (2.14). The surface integral can be written as

$$\int_{\partial \mathcal{P}} t \, dA = \int_{\partial \mathcal{P}} (\sigma \cdot n) \, dA = \int_{\mathcal{P}} \text{div}[\sigma] \, dV \, . \tag{2.16}$$

By making use of this result in (2.15), we end up with

$$\int_{\mathcal{P}} \rho \, \dot{\boldsymbol{v}} dV = \int_{\mathcal{P}} (\rho \, \boldsymbol{b} + \mathrm{div}[\boldsymbol{\sigma}]) \, dV \,. \tag{2.17}$$

Localizing the part $\mathcal{P}$ to an infinitesimal volume

$$\lim_{\mathcal{P} \to dV} \int_{\mathcal{P}} (\rho \, \dot{\boldsymbol{v}} - \mathrm{div}[\boldsymbol{\sigma}] - \rho \, \boldsymbol{b}) \, dV = 0 \,, \tag{2.18}$$

we arrive at the local form of the balance of linear momentum equation

$$\rho \, \dot{\boldsymbol{v}} = \mathrm{div}[\boldsymbol{\sigma}] + \rho \, \boldsymbol{b} \,. \tag{2.19}$$

Conservation of Angular Momentum

Inserting the mechanical couple expression $(2.7)_2$ into $(2.9)_3$, we obtain

$$\frac{d}{dt} \boldsymbol{\mathcal{D}}_0 = \frac{d}{dt} \int_{\mathcal{P}} \boldsymbol{x} \times \rho \boldsymbol{v} \, dV = \int_{\mathcal{P}} \boldsymbol{x} \times \rho \boldsymbol{b} \, dV + \int_{\partial \mathcal{P}} \boldsymbol{x} \times \boldsymbol{t} \, dA \tag{2.20}$$

Transforming the surface integral into a volume integral

$$\int_{\partial \mathcal{P}} \boldsymbol{x} \times \boldsymbol{t} \, dA = \int_{\mathcal{P}} \boldsymbol{\epsilon} : \boldsymbol{\sigma}^T \, dV + \int_{\mathcal{P}} \boldsymbol{x} \times \mathrm{div}[\boldsymbol{\sigma}] \, dV \,, \tag{2.21}$$

and by inserting this result into (2.20), the conservation of angular momentum equation becomes

$$\frac{d}{dt} \int_{\mathcal{P}} \boldsymbol{x} \times \rho \boldsymbol{v} \, dV = \int_{\mathcal{P}} (\boldsymbol{v} \times \rho \boldsymbol{v} + \boldsymbol{x} \times \rho \dot{\boldsymbol{v}}) \, dV \,,$$
$$= \int_{\mathcal{P}} \boldsymbol{x} \times \rho \boldsymbol{b} \, dV + \int_{\mathcal{P}} \boldsymbol{x} \times \mathrm{div}[\boldsymbol{\sigma}] \, dV + \int_{\mathcal{P}} \boldsymbol{\epsilon} : \boldsymbol{\sigma}^T \, dV \,. \tag{2.22}$$

Making use of the conservation of mass equation (2.14) and the equality $\boldsymbol{v} \times \boldsymbol{v} = \boldsymbol{0}$ in (2.22), we end up with

$$\int_{\mathcal{P}} (\boldsymbol{x} \times (\rho \, \boldsymbol{a} - \mathrm{div}[\boldsymbol{\sigma}] - \rho \, \boldsymbol{b}) \, dV + \int_{\mathcal{P}} \boldsymbol{\epsilon} : \boldsymbol{\sigma}^T \, dV = \boldsymbol{0} \,. \tag{2.23}$$

The conservation of linear momentum equation in (2.19) nullifies the term in parantheses with $\dot{\boldsymbol{v}} = \boldsymbol{a}$. Hence, the first term on the left hand side of (2.23) vanishes. Therefore, the final reduced form of the equation becomes

$$\lim_{\mathcal{P} \to dV} \int_{\mathcal{P}} \boldsymbol{\epsilon} : \boldsymbol{\sigma}^T \, dV = \boldsymbol{0} \quad \Longleftrightarrow \quad \boldsymbol{\epsilon} : \boldsymbol{\sigma}^T = \boldsymbol{0} \,. \tag{2.24}$$

Since $\epsilon_{123} = \epsilon_{231} = \epsilon_{312} = 1$ and $\epsilon_{132} = \epsilon_{213} = \epsilon_{321} = -1$, the equality (2.24) implies $\sigma_{23} = \sigma_{32}, \sigma_{31} = \sigma_{13}, \sigma_{12} = \sigma_{21}$, or simply

$$\boldsymbol{\sigma} = \boldsymbol{\sigma}^T. \tag{2.25}$$

That is, the conservation of angular momentum implies that the stress tensor is symmetrical.

Conservation of Energy *(1st Law of Thermodynamics)*

Recall the global form of conservation of energy in equation (2.9),

$$\frac{d}{dt}[\mathcal{K} + \mathcal{E}] = \mathcal{P} + \mathcal{Q},$$

where $\mathcal{K}$, $\mathcal{E}$, $\mathcal{P}$, and $\mathcal{Q}$ represent the kinetic energy, internal energy, mechanical power, and thermal power, respectively. While the left hand side of the equality is the rate of kinetic and internal energy of $\mathcal{P} \subset \mathcal{B}$, the right hand side represents the mechanical and thermal power terms. By using (2.7) and (2.8), the explicit form of the conservation of energy can be written as

$$\frac{d}{dt}\left[\int_{\mathcal{P}} \frac{1}{2}\rho\,\boldsymbol{v}\cdot\boldsymbol{v}\,dV + \int_{\mathcal{P}}\rho\,e\,dV\right]$$
$$= \int_{\mathcal{P}}\rho\,\boldsymbol{b}\cdot\boldsymbol{v}\,dV + \int_{\partial\mathcal{P}}\boldsymbol{t}\cdot\boldsymbol{v}\,dA + \int_{\mathcal{P}}\rho\,r\,dV - \int_{\partial\mathcal{P}}h\,dA, \tag{2.26}$$

where all the terms are in the volume integral except for the terms with the traction vector and the heat flux. Transforming the surface contribution of the mechanical power term into a volume integral, we obtain

$$\int_{\partial\mathcal{P}}\boldsymbol{v}\cdot\boldsymbol{t}\,dA = \int_{\partial\mathcal{P}}\boldsymbol{v}\cdot\boldsymbol{\sigma}\cdot\boldsymbol{n}\,dA = \int_{\mathcal{P}}(\nabla\boldsymbol{v}:\boldsymbol{\sigma} + \boldsymbol{v}\cdot\mathrm{div}[\boldsymbol{\sigma}])\,dV \tag{2.27}$$

where $\nabla\boldsymbol{v}:\boldsymbol{\sigma}$ can be expressed as the stress power term as follows

$$\nabla\boldsymbol{v}:\boldsymbol{\sigma} = \boldsymbol{\sigma}:\nabla\boldsymbol{v} = \boldsymbol{\sigma}:\mathrm{sym}(\nabla\boldsymbol{v}) = \boldsymbol{\sigma}:\dot{\boldsymbol{\varepsilon}}. \tag{2.28}$$

The equality $\dot{\boldsymbol{\varepsilon}} = \mathrm{sym}(\nabla\boldsymbol{v})$ is derived from (2.4). Then, the volume transformation equation becomes

$$\int_{\mathcal{P}}(\boldsymbol{\sigma}:\dot{\boldsymbol{\varepsilon}} + \boldsymbol{v}\,\mathrm{div}[\boldsymbol{\sigma}])\,dV. \tag{2.29}$$

25

Similar to the surface contribution of the mechanical power term, the surface contribution of the thermal power can be recast into a volume integral through the Cauchy's theorem (2.6)

$$\int_{\partial\mathcal{P}} h \, dA = \int_{\partial\mathcal{P}} \boldsymbol{q} \cdot \boldsymbol{n} \, dA = \int_{\mathcal{P}} \text{div}[\boldsymbol{q}] \, dV \,. \tag{2.30}$$

Incorporating the results (2.29) and (2.30) in the conservation of energy, we arrive at

$$\int_{\mathcal{P}} \rho \boldsymbol{v} \cdot \dot{\boldsymbol{v}} \, dV + \int_{\mathcal{P}} \rho \dot{e} \, dV = \int_{\mathcal{P}} \rho \left(\boldsymbol{b} \cdot \boldsymbol{v} + \boldsymbol{\sigma} : \dot{\boldsymbol{\varepsilon}} + \boldsymbol{v} \, \text{div}[\boldsymbol{\sigma}] \right) \, dV$$
$$+ \int_{\mathcal{P}} \left(\rho \, r - \text{div}[\boldsymbol{q}] \right) \, dV \,. \tag{2.31}$$

Insertion of (2.27) and (2.30) into (2.31) leads us to

$$\int_{\mathcal{P}} \boldsymbol{v} \cdot \left(\rho \, \boldsymbol{a} - \text{div}[\boldsymbol{\sigma}] - \rho \, \boldsymbol{b} \right) dV + \int_{\mathcal{P}} \left(\rho \dot{e} - \boldsymbol{\sigma} : \dot{\boldsymbol{\varepsilon}} - \rho \, r + \text{div}[\boldsymbol{q}] \right) dV = 0 \,. \tag{2.32}$$

Incorporation of the conservation of linear momentum (2.18) in (2.32) leads us to the balance of energy equation

$$\int_{\mathcal{P}} \left(\rho \dot{e} - \boldsymbol{\sigma} : \dot{\boldsymbol{\varepsilon}} - \rho \, r + \text{div}[\boldsymbol{q}] \right) dV \tag{2.33}$$

whose localization leads us to the local form of the conservation of energy

$$\rho \dot{e} = \boldsymbol{\sigma} : \dot{\boldsymbol{\varepsilon}} + \rho \, r - \text{div}[\boldsymbol{q}] \,. \tag{2.34}$$

The local energy conservation equation can be further elaborated to obtain the transient heat conduction equation. For this, the reader is referred to Section 3.5.

While the balance of linear momentum governs the mechanical behavior of a body, the conservation of energy describes its thermal response. In thermomechanical problems, these two equations are coupled through constitutive equations and solved simultaneously.

Conservation of Entropy *(2nd Law of Thermodynamics)*

Substituting $(2.7)_6$ into $(2.9)_5$, we end up with

$$\Gamma := \int_{\mathcal{P}} \rho \, \gamma \, dV = \frac{d}{dt} (\mathcal{H}) - \mathcal{S}$$
$$= \frac{d}{dt} \int_{\mathcal{P}} \rho \, \eta \, dV - \int_{\mathcal{P}} \rho \frac{r}{\theta} \, dV + \int_{\partial\mathcal{P}} \frac{h}{\theta} \, dA \geq 0 \,. \tag{2.35}$$

The surface contribution to the entropy power is transformed from surface integral into a volume integral as

$$\int_{\partial\mathcal{P}} \frac{h}{\theta}\, dA = \int_{\partial\mathcal{P}} \frac{\boldsymbol{q}\cdot\boldsymbol{n}}{\theta}\, dA\,,$$

$$= \int_{\mathcal{P}} \left(\frac{1}{\theta}\, \mathrm{div}[\boldsymbol{q}] - \frac{1}{\theta^2}\, \boldsymbol{q}\cdot\nabla\theta \right) dV\,. \tag{2.36}$$

Inserting (2.36) into (2.35), we get

$$\int_{\mathcal{P}} \rho\,\gamma\, dV = \int_{\mathcal{P}} \rho\,\dot{\eta}\, dV - \int_{\mathcal{P}} \rho\,\frac{r}{\theta}\, dV + \int_{\mathcal{P}} \left(\frac{1}{\theta}\, \mathrm{div}[\boldsymbol{q}] - \frac{1}{(\theta)^2}\, \boldsymbol{q}\cdot\nabla\theta \right) dV\,. \tag{2.37}$$

Localizing the global form (2.37)

$$\lim_{\mathcal{P}\to dV} \int_{\mathcal{P}} \left(\rho\,\gamma - \rho\,\dot{\eta} + \rho\,\frac{r}{\theta} - \frac{1}{\theta}\, \mathrm{div}[\boldsymbol{q}] - \frac{1}{(\theta)^2}\, \boldsymbol{q}\cdot\nabla\theta \right) dV = 0\,, \tag{2.38}$$

we obtain the local form of conservation of entropy as

$$\rho\,\gamma = \rho\,\dot{\eta} + \frac{1}{\theta}\,(\rho r - \mathrm{div}[\boldsymbol{q}]) - \frac{1}{\theta^2}\, \boldsymbol{q}\cdot\nabla\theta \geq 0\,. \tag{2.39}$$

The local forms of the conservation laws are summarized as followed.

(i)   Mass $\dot{\rho} = 0$

(ii) LinearMomentum $\rho\,\boldsymbol{a} = \mathrm{div}[\boldsymbol{\sigma}] + \rho\,\boldsymbol{b}$

(iii) AngularMomentum $\boldsymbol{\sigma} = \boldsymbol{\sigma}^T$

(iv) Energy $\rho\dot{e} = \boldsymbol{\sigma}:\dot{\boldsymbol{\varepsilon}} + \rho\,r - \mathrm{div}[\boldsymbol{q}]$

(v)   Entropy $\rho\,\gamma = \rho\,\dot{\eta} + \dfrac{1}{\theta}\,(\rho r - \mathrm{div}[\boldsymbol{q}]) - \dfrac{1}{\theta^2}\, \boldsymbol{q}\cdot\nabla\theta \geq 0$

2.4   Dissipation

The dissipation, $\mathcal{D}$, is defined as the product of the volume-specific entropy production rate (2.39) and the absolute temperature

$$\mathcal{D} := \theta\rho\gamma \geq 0 \quad \text{with} \quad \theta \geq 0 \tag{2.40}$$

Making use of the conservation of energy (2.34) and the conservation of entropy (2.39) in (2.40), we obtain

$$\mathcal{D} := \theta\,\rho\,\gamma \;=\; \rho\theta\dot{\eta} - (\rho r - \mathrm{div}[\boldsymbol{q}]) - \frac{1}{\theta}\boldsymbol{q}\cdot\nabla\theta \geq 0\,,$$

$$= \; \rho\theta\dot{\eta} - (\rho\dot{e} - \boldsymbol{\sigma}:\dot{\boldsymbol{\varepsilon}}) - \frac{1}{\theta}\boldsymbol{q}\cdot\nabla\theta \geq 0\,,$$

$$\mathcal{D} \;=\; \boldsymbol{\sigma}:\dot{\boldsymbol{\varepsilon}} - \rho\,\dot{e} + \rho\,\theta\,\dot{\eta} - \frac{1}{\theta}\boldsymbol{q}\cdot\nabla\theta \geq 0\,. \tag{2.41}$$

The latter inequality is called the *Clasius-Duhem Inequality* (CDI) and consists of two parts: the local (intrinsic) dissipation $\mathcal{D}_{loc}$ and the dissipation because of the heat conduction $\mathcal{D}_{con}$

$$
\begin{aligned}
\mathcal{D}_{loc} &= \boldsymbol{\sigma} : \dot{\boldsymbol{\varepsilon}} - \rho\,\dot{e} + \rho\,\theta\,\dot{\eta} \geq 0\,, \\
\mathcal{D}_{con} &= -\frac{1}{\theta}\,\boldsymbol{q} \cdot \nabla\theta \geq 0\,.
\end{aligned}
\tag{2.42}
$$

The first inequality is called the *Clasius-Planck Inequality* (CPI) and the latter is the *Fourier Inequality* (FI).

Introducing the Helmholtz free energy $\hat{\Psi}$ through the of Legendre transformation

$$
\hat{\Psi} := e - \theta\,\eta
\tag{2.43}
$$

the following alternative representation of CPI is arrived

$$
\mathcal{D}_{loc} = \boldsymbol{\sigma} : \dot{\boldsymbol{\varepsilon}} - \rho\,\dot{\hat{\Psi}} + \rho\,\eta\,\dot{\theta} \geq 0
\tag{2.44}
$$

In thermodynamics of materials, constitutive equations that fulfill the Clausius-Planck and Fourier inequalities (3.6) are said to be thermodynamically consistent. For thermoelasticity, the local dissipation vanishes identically and the CPI becomes an equality

$$
\mathcal{D}_{loc} = \boldsymbol{\sigma} : \dot{\boldsymbol{\varepsilon}} - \rho\,\dot{\hat{\Psi}} + \rho\,\eta\,\dot{\theta} = 0\,,
\tag{2.45}
$$

which implies $\hat{\Psi} = \hat{\Psi}(\boldsymbol{\varepsilon}, \theta)$.

CHAPTER 3

CONSTITUTIVE EQUATIONS

In Chapter 2, the global balance laws and their local forms have been derived. These resulting field equations are valid for all closed thermomechanical bodies, but they are insufficient to describe the response of early-age concrete to the acting forces and thermal loads. In order to provide a specific definition of the material behavior, constitutive equations are required. The aim of this chapter is to introduce the constitutive equations of the coupled initial boundary-value problem of early-age concrete thermomechanics within the framework of Theory of Reactive Porous Media [17, 65, 66, 67]. After introducing the essential governing differential equations of the problem, mechanical and thermal material properties are defined based on the state variables. At the end of the chapter, special forms of the material coefficients are given.

3.1 Theory of Reactive Porous Media

Concrete is one of the most commonly used construction materials in structures like dams, bridges, viaducts, ports, tunnels, etc., which are subjected to different environmental conditions. In order to simulate the behavior of these concrete structures, a coupled thermomechanical model is required.

During concrete hardening, several different physical and chemical phenomena occur. Despite the complexity of this process, a coupled chemo-thermo-mechanical model can clarify the hardening and hydration. As a result of exothermic nature of cement hydration, the heat of hydration arises and causes an increase of the temperature

29

field in structures. This increase results in undesired irregular temperature variations throughout a structure's body depending on the thermal boundary conditions. Especially in concrete dams, power plants, foundations, bridge and viaduct piers, which are generally called mass concrete. Owing to the low thermal conductivity of concrete, it is not easy to convect the heat of hydration from the surface of structures to ambient. Therefore, in the interior regions of mass concrete high temperature increases occur, and this, in turn, causes thermal expansions. These volume changes and external restraints of concrete structure lead to the development of tensile stress. The excessive amount of the tensile stress may result in local cracks.

As explained in Chapter 1, cement consists 4 fundamental minerals; calcium silicates (C_2S, C_3S), a calcium aluminate (C_3A) and a calcium aluminoferrite (C_4AF). These minerals react with water during the hydration process and create different hydration products. The products of aluminates' hydration vary with the amount of sulfate they include where ettringite is referred to as high-sulfate ($C_6A\bar{S}_3H_{32}$) and monosulfate is also called as low-sulfate ($C_4A\bar{S}H_{18}$). On the other hand, the hydration of the silicates constitutes calcium hydroxide (CH) and calcium silica hydrate (CSH). Because of different reactivity of these formations, the chemical system is simplified as clinker hydration. Temperature and the degree of hydration are assumed as the two essential variables of this closed thermo-chemical model and the free energy is formulated in terms of these variables. As a consequence of hydration, the dissipated energy grows into a heat source in the transient heat conduction equation (2.34). The time evolution of the mechanical properties of concrete during hydration is called aging and this phenomenon is modelled with the concept of the degree of aging. To complete the model, the material parameters must be determined. This is done with the help of different experimental data.

3.2 The Principal Kinematics of the Chemo-Thermo-Mechanical Problem

The general kinematics of continuum mechanics is described in Chapter 2. In this section, general kinematics is defined for the coupled problem. Let $\mathcal{B}$ be the referance position of a concrete body, which has material points in coordinates of $x \in \mathcal{B}$ at time of $t \in \mathbb{R}_+$ and the displacement of these points is denoted by $u(x, t)$. In the

model, coupled chemical and thermal phenomena initiate the mechanical deformations. Under this condition, small strain theory is assumed and the linear strain tensor $\varepsilon(\boldsymbol{x}, t)$ is used. The other external variable is the temperature field and is denoted by $\theta(\boldsymbol{x}, t)$ while the main indicator of the hydration process would be expressed by the degree of hydration $\xi(\boldsymbol{x}, t)$. The latter enters the formulation as an internal field.

3.3 Thermodynamical Structure of the Model

In order to describe the local chemo-thermo-mechanical behavior of the hardening concrete at time $t \in \mathbb{R}_+$, we need to know the displacement, thermal and hydration fields. Therefore, the strain tensor $\varepsilon(\boldsymbol{x}, t)$, absolute temperature $\theta(\boldsymbol{x}, t)$ and the degree of hydration $\xi(\boldsymbol{x}, t)$ are the key fields. These state variables govern the Helmholtz free energy, which is chosen as the thermomechanical potential

$$\Psi = \hat{\Psi}(\varepsilon, \theta, \xi) \,. \tag{3.1}$$

When the coupled chemo-thermo-mechanical effects are taken into account, the Helmholtz free energy function will be considered as,

$$\hat{\Psi}(\varepsilon, \theta, \xi) = \hat{W}(\varepsilon, \theta, \xi) + \hat{V}(\theta) + \hat{L}(\theta, \xi) + \hat{H}(\xi) \,, \tag{3.2}$$

where the thermoelastic energy $\hat{W}(\varepsilon, \theta, \xi)$ takes thermal effects and the effect of aging of concrete on mechanical energy into consideration, the thermal energy function $\hat{V}(\theta)$ represents completely thermal energy that is stored in concrete; $\hat{L}(\theta, \xi)$ accounts for chemo-thermal effects in concrete and depends on temperature and the degree of hydration. $\hat{H}(\xi)$ is the chemical energy.

Therefore, according to the second law of thermodynamics, the instrinsic dissipation for the non-isothermal problems can be introduced as

$$\mathcal{D}_{\text{int}} = \boldsymbol{\sigma} : \dot{\varepsilon} - \dot{\Psi} - \eta \dot{\theta} \geq 0 \,. \tag{3.3}$$

In this inequality, the stress tensor is denoted by $\boldsymbol{\sigma}$ and η represents the entropy per unit volume. When the dependence of the Helmholtz free energy on the tensor strain, the temperature, and the degree of hydration is taken into account, (3.3) becomes

$$\mathcal{D}_{\text{int}} = (\boldsymbol{\sigma} - \partial_{\varepsilon} \hat{\Psi}) : \dot{\varepsilon} - (\eta + \partial_{\theta} \hat{\Psi}) \dot{\theta} - \partial_{\xi} \hat{\Psi} : \dot{\xi} \geq 0 \,. \tag{3.4}$$

According to the methodology of the Coleman and Gurtin [19], the values in parenthesis in (3.4) are expected to be zero for arbitrary time rate of the strain tensor and the absolute temperature. The Helmholtz free energy then acts as a potential for the stress tensor $\boldsymbol{\sigma}$ and the entropy η through the following equations

$$\boldsymbol{\sigma} = \partial_{\boldsymbol{\varepsilon}} \hat{\Psi}(\boldsymbol{\varepsilon}, \theta, \xi), \qquad \eta = -\partial_{\theta} \hat{\Psi}(\boldsymbol{\varepsilon}, \theta, \xi). \tag{3.5}$$

Incorporating the results (3.5) in (3.4), the Clausius-Planck Inequality reduces to the following form

$$\mathcal{D}_{\text{int}} = \hat{A}_{\xi} \dot{\xi} \geq 0, \tag{3.6}$$

where $\hat{A}_{\xi} := -\partial_{\xi} \hat{\Psi}(\boldsymbol{\varepsilon}, \theta, \xi)$ represents the *chemical affinity*, an energy-conjugate variable of the degree of hydration. One of the key equations of the coupled chemo-thermal problem for a closed thermodynamical system is the evolution of the degree of hydration. This can be described as a thermally activated process through an Arrhenius-type differential equation

$$\dot{\xi} = \frac{\hat{A}_{\xi}}{\hat{\eta}_{\xi}} \exp\left(-\frac{E_a}{R\theta}\right) \tag{3.7}$$

In this equation $\hat{\eta}_{\xi}(\xi)$, E_a, and R denote the viscosity, which controls the rate of reaction and depends on the degree of hydration, the activation energy and the universal gas coefficient, respectively. This new definition for the evolution of the degree of hydration enters the Clasius-Planck Inequality (3.6) and it takes its final reduced form as

$$\mathcal{D}_{\text{int}} = \frac{\hat{A}_{\xi}^2}{\hat{\eta}_{\xi}} \exp\left(-\frac{E_a}{R\theta}\right) \geq 0. \tag{3.8}$$

In order to fulfill the Clasius-Planck Inequality (3.6), $\hat{\eta}_{\xi}(\xi)$ viscosity function must be positive ($\hat{\eta}_{\xi} \geq 0$). Then, the suggested model can be said to be thermodynamically consistent. The Fourier inequality explains the heat conduction limiting part of the second law of thermodynamics

$$\mathcal{D}_{con} = -\frac{1}{\theta} \hat{\boldsymbol{q}} \cdot \nabla_x \theta \geq 0. \tag{3.9}$$

that can be satisfied identically for the positive values of the coefficient of thermal conductivity with Fourier-type $\hat{\boldsymbol{q}} = -k \nabla_x \theta$ isotropic heat conduction model; that is, $\mathcal{D}_{con} = k \theta^{-1} \|\nabla_x \theta\|^2 \geq 0 \quad \forall k \geq 0$.

3.4 Balance Laws of Coupled Chemo-Thermo-Mechanical System

As discussed in Chapter 2, the essential equations of chemo-thermo-mechanics are the conservation of linear momentum (2.18) and the conservation of energy (2.34). Under quasi-static conditions, inertia effect can be neglected and the conservation of linear momentum law boils down to

$$\text{div}[\boldsymbol{\sigma}] + \boldsymbol{b} = \boldsymbol{0} \tag{3.10}$$

where $\boldsymbol{b}$ represents volume-specific body force. The conservation of energy, which is also known as the first law of thermodynamics can be introduced as the summation of mechanical power, which is the change of time rated internal energy $\mathcal{P} := \boldsymbol{\sigma} : \dot{\boldsymbol{\varepsilon}}$, and thermal power $\mathcal{Q} := -\text{div}[\hat{\boldsymbol{q}}] + r$,

$$\dot{e} = \mathcal{P} + \mathcal{Q}, \tag{3.11}$$

where e denotes the volume-specific internal energy. When the results in (3.5) and the Legendre relation of $e := \Psi + \theta\eta$ between internal energy and Helmholtz free energy are incorporated in (3.11), the conservation of energy can be expressed as

$$\theta\dot{\eta} = \mathcal{D}_{\text{int}} + \mathcal{Q}. \tag{3.12}$$

Recall that entropy is defined as $\eta = -\partial_\theta \hat{\Psi}(\varepsilon, \theta, \xi)$ in (3.5). If we exploit its dependency on the external and internal state variables, the transient heat conduction equation describing the evolution of the temperature field is obtained as

$$c\dot{\theta} = \mathcal{Q} + \mathcal{D}_{\text{int}} + \mathcal{H}_{\text{mech}} + \mathcal{H}_{\text{chem}}. \tag{3.13}$$

In this equality, $c := -\theta\partial_{\theta\theta}^2\hat{\Psi}$, $\mathcal{H}_{\text{mech}} := \theta\partial_\theta\boldsymbol{\sigma} : \dot{\boldsymbol{\varepsilon}}$ and $\mathcal{H}_{\text{chem}} := \theta\partial_{\xi\theta}^2\hat{\Psi}\dot{\xi}$ stand for the specific heat, thermoelastic heating and chemical heating, respectively. $\mathcal{H}_{\text{chem}}$ is the product of exothermic hydration reaction and when it is compared with the internal energy loss $\mathcal{D}_{\text{int}}$ and thermoelastic heat $\mathcal{H}_{\text{mech}}$, the latter two terms can be neglected. To this respect, if the hydration effects are taken into consideration and for the hardening concrete, the conservation of energy equation becomes.

$$c\dot{\theta} = \mathcal{Q} + \mathcal{H}_{\text{chem}} \tag{3.14}$$

This new form is valid for non-adiabatic systems. Under adiabatic conditions, i.e. as the system is insulated, the thermal power term vanishes ($\mathcal{Q} = 0$) and the transient

heat conduction equation becomes an ordinary differential equation

$$c\,\dot{\theta} = \mathcal{H}_{\text{chem}}\,. \tag{3.15}$$

The solution of the latter can be used to estimate the changes in the local temperature field.

3.5 Specific Constitutive Equations

Formerly explained conservation of linear momentum (3.10) and the conservation of energy (3.14) equations are coupled through constitutive equations. In this section, specific parts of Helmholtz free energy function are introduced. We assume the specific form of thermoelastic energy function as

$$\hat{W}(\boldsymbol{\varepsilon}, \theta, \xi) = \frac{\hat{\kappa}(\xi)}{2}[\text{tr}(\boldsymbol{\varepsilon})]^2 - \hat{\kappa}(\xi)\alpha\,\text{tr}(\boldsymbol{\varepsilon})(\theta - \theta_0) + \hat{\mu}(\xi)\,\text{dev}(\varepsilon):\text{dev}(\varepsilon) \tag{3.16}$$

where $\hat{\kappa}(\xi)$ and $\hat{\mu}(\xi)$, α and θ_0 denote the degree of hydration based bulk and shear moduli, the thermal expansion coefficient, and the initial temperature value, respectively. This specific form considers the thermal effects on the mechanical behavior of concrete. The purely thermal part of the Helmholtz free energy function $\hat{V}(\theta)$ models the rigid thermal energy storage

$$\hat{V}(\theta, \xi) = \hat{c}(\xi)[\theta - \theta_0\,\ln(\theta/\theta_0)]\,. \tag{3.17}$$

The thermochemical effects are modeled by the energy function

$$\hat{L}(\theta, \xi) = \hat{Q}(\xi)\,\ln(\theta/\theta_0)\,, \tag{3.18}$$

where the heat source $\hat{Q}(\xi)$ refers to the amount of heat per unit volume, which is released during the hydration process and modelled as a function of the degree of hydration

$$\hat{Q}(\xi) = Q_\xi\,\xi\,. \tag{3.19}$$

If it is considered that the degree of hydration ranges between 0 and 1, this equation clarifies that the material coefficient Q_ξ as the arising amount of heat at unit hydration. The last part of the Helmholtz free energy models the purely chemical effects

$$\hat{H}(\xi) = \frac{1}{3}\,k_\xi\,\xi^3 + \frac{1}{2}\,(A_{\xi_0}/\xi_\infty)\xi^2 - A_{\xi_0}\xi\,. \tag{3.20}$$

where k_ξ and A_{ξ_0} are material coefficients and ξ_∞ is the final (steady-state) value of the degree of hydration. The final value of the degree of hydration is related to the water - cement ratio of the concrete mixture. Pantazopoulo and Mills [57] introduced a water - cement ratio based function of the final value of degree of hydration

$$\xi_\infty = \frac{1.031 \, \text{w/c}}{0.194 + \text{w/c}} \, . \tag{3.21}$$

The stress tensor $\boldsymbol{\sigma}$ and the chemical affinity A_ξ can be derived with the combination of the constitutive equations and the equations in Section 3.3. We then have the specific expressions of the stress tensor

$$\boldsymbol{\sigma} = \hat{\kappa}(\xi)[(\text{tr}(\boldsymbol{\varepsilon}) - \alpha(\theta - \theta_0))] \, \mathbf{1} + 2\hat{\mu}(\xi) \, \text{dev}(\boldsymbol{\varepsilon}) \, , \tag{3.22}$$

and the chemical affinity

$$A_\xi = \kappa_\xi \left(\frac{A_{\xi_0}/k_\xi}{\xi_\infty} + \xi \right) (\xi_\infty - \xi) \, . \tag{3.23}$$

Observe that in the definition of the chemical affinity $A_\xi := -\partial_\xi \hat{\Psi} = -\partial_\xi \hat{W} - \partial_\xi \hat{L} - \partial_\xi \hat{H}$, the contribution of thermoelastic $(-\partial_\xi \hat{W})$ and the chemothermal $(-\partial_\xi \hat{L})$ parts are ignored when compared with the contribution of chemical energy $(-\partial_\xi \hat{H})$ and the assumption of $A_\xi := -\partial_\xi \hat{\Psi} \approx -\partial_\xi \hat{H}$ is admitted. Recall evolution of the degree of hydration in (3.7),

$$\dot{\xi} = \frac{\hat{A}_\xi}{\hat{\eta}_\xi} \exp \left(-\frac{E_a}{R\theta} \right) \, .$$

When the latter definition of the chemical affinity is used in the evolution equation of the degree of hydration, we obtain the following form

$$\dot{\xi} = \frac{k_\xi}{\hat{\eta}_\xi} \left(\frac{A_{\xi_0}/k_\xi}{\xi_\infty} + \xi \right) (\xi_\infty - \xi) \exp \left(-\frac{E_a}{R\theta} \right) \, . \tag{3.24}$$

In this equation, $\hat{\eta}_\xi(\xi)$ is introduced as an increasing function of the degree of hydration [17],

$$\hat{\eta}_\xi(\xi) = \eta_{\xi_0} \exp \left(\eta \frac{\xi}{\xi_\infty} \right) \, , \tag{3.25}$$

where η_{ξ_0} and η are material constants. In chemically closed porous media, $\hat{\eta}_\xi(\xi)$ represents the diffusion of water. For the chemical heating $\mathcal{H}_{\text{chem}} := \theta \partial_{\xi\theta}^2 \hat{\Psi} \dot{\xi}$ in conservation of energy function (3.14), if we consider the contribution of the thermochemical energy is far bigger than that of the thermoelastic one, the chemical heating simplifies to $\mathcal{H}_{\text{chem}} := Q_\xi \dot{\xi}$. For the adiabatic case, the temperature evolution becomes

$$c\dot{\theta} = Q_\xi \dot{\xi} \, , \tag{3.26}$$

and integrating it over time the change in the absolute temperature during hydration can be calculated as

$$\theta - \theta_0 = \frac{Q_\xi}{c} \left[\xi(t) - \xi_0\right] . \tag{3.27}$$

3.6 Aging Equations

It is necessary to clarify the effects of hydration on the behavior of concrete hardening. During hydration, durability properties and mechanical behavior of concrete change. To model this alteration, we use the aging variable $\chi = \hat{\chi}(\theta, \xi)$, which takes into account of the effect of ambient temperature. The compressive strength of concrete can be introduced in terms of the ultimate strength f_c^∞ under isothermal conditions

$$f_c(\chi) = \hat{\chi} f_c^\infty . \tag{3.28}$$

The evolution of the aging variable [17] is described by,

$$\dot{\chi} = \hat{\lambda}_\theta \hat{\lambda}_\xi \dot{\xi} , \tag{3.29}$$

with functions $\hat{\lambda}_\theta$ and $\hat{\lambda}_\xi$ defined as

$$\hat{\lambda}_\theta := \left(\frac{\theta_{\max} - \theta}{\theta_{\max} - \theta_r}\right)^{n_\theta} , \qquad \hat{\lambda}_\xi = A_f \xi + B_f \tag{3.30}$$

where $\theta_{\max}$ denotes the maximum temperature, n_θ is a material constant and A_f and B_f control the variation of the degree of aging with the degree of hydration. According to CEB-FIP Model Code (1990), concrete's tensile strength f_t and its modulus of elasticity E_c can be calculated based on the compressive strength in megapascals.

$$f_t(\chi) = 1.40 \left(f_c(\chi)/10\right)^{2/3} \qquad [\text{MPa}] \tag{3.31}$$

$$E_c(\chi) = 2.15 \cdot 10^4 \left(f_c(\chi)/10\right)^{1/3} \qquad [\text{MPa}] \tag{3.32}$$

The material parameters of the constitutive and aging equations are listed in Table 3.1 with reference to the equations where they appear. The first eight parameters are for constitutive equations and the others are required for defining the aging equations.

In the next chapter, the specific values of parameters in Table 3.1 are going to be determined by the help of experimental studies, which are compared with the numerical simulations.

3.7 Special Forms of Material Parameters

As a consequence of cement hydration and its end products, thermal and mechanical material parameters of concrete vary. This section outlines the specific forms of the thermal and mechanical material parameters as a function of the degree of hydration.

3.7.1 Thermal Material Parameters

There are three thermal material parameters that have an important effect on concrete: the specific heat capacity, the thermal conductivity and the coefficient of thermal expansion.

The specific heat can be defined as the amount of energy required per unit mass to change the temperature by 1 Kelvin. For lower values of specific heat, it will be easier to increase the temperature of concrete and vice versa. Because of the thermally vulnerable behavior of concrete, specific heat becomes a fundamental thermal material parameter. The content of cement and the composition of mixture materials play an important role on the evaluation of the specific heat. Any thermal or mechanical

Table 3.1: Material Parameters of Constitutive and Aging Parameters

Parameter	Description	Equation
c	Coefficient of specific heat	(3.13)
θ_0	Initial temperature	(3.16, 3.17, 3.18)
Q_ξ	Latent heat of hydration	(3.19, 3.26, 3.27)
ξ_∞	Ultimate degree of hydration	(3.21, 3.23, 3.24, 3.25)
$k_{\xi_\infty}/\eta_{\xi_0}$	Hydration parameter	(3.24, 3.25)
η	Viscosity	(3.25)
A_{ξ_0}/k_ξ	Hydration parameter	(3.24, 3.25)
E_a/R	Normalized activation energy	(3.7, 3.24)
f_c^∞	Ultimate compressive strength	(3.28)
θ_r	Reference temperature	$(3.30)_1$
$\theta_{\max}$	Maximum temperature	$(3.30)_2$
n_θ	Temperature base parameter	$(3.30)_1$
A_f, B_f	Aging coefficients	$(3.30)_2$

change in concrete will change the specific heat capacity. The effects of these thermal and mechanical fields on the coefficient of specific heat have been investigated in different experimental studies [23, 40, 62].

According to De Schutter [21], the specific heat decreases linearly with the increase of the degree of hydration. He introduced a hydration-based specific heat equation for concrete

$$c\left(\xi\right) = c_{\infty}\left(1.15 - 0.15\,\xi\right) \tag{3.33}$$

This equation is valid only for concrete with normal weight gravel and c_{∞} denotes specific heat of hardened concrete. For hardened concrete with normal weight aggregate, the coefficient of specific heat capacity ranges between 800 and 900 $\mathrm{m^2/(s^2\,K)}$. A typical specific heat capacity evolution curve is depicted in Figure 3.1.
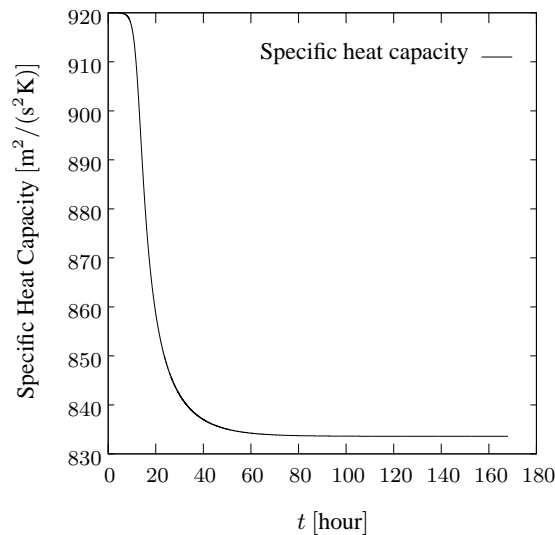
Figure 3.1: Coefficient of specific heat capacity curve of normal strength concrete with % 20 fly ash. Curve is depicted according to (3.33) with $c_{\infty} = 800\,[\mathrm{m^2/(s^2\,K)}]$

The other thermal material parameter, thermal conductivity, controls uniform heat flow through a unit thickness of concrete between its opposite surfaces. Unit of thermal conductivity is $\mathrm{W/(m\,K)}$. Lixia et al. [49] designed an experiment to determine the coefficient of thermal conductivity and to understand the importance of concrete mixture materials on this coefficient. Although it is widely assumed that the coefficient of thermal conductivity is constant, Ruiz et al. [59] and Shin et al. [62] present linear and nonlinear formulations of the thermal conductivity of concrete, respec-

38

tively. Moreover, Jeong and Kim [38] suggest that the thermal conductivity of concrete decreases as the degree of hydration increases with regard to their experimental study on concrete pavements. Ruiz's thermal conductivity equation is

$$k\left(\xi\right) = k_{\infty}\left(1.33 - 0.33\,\xi\right), \tag{3.34}$$

where k_{∞} is the ultimate thermal conductivity of hardened concrete.

In this study, we assume that concrete is a homogenous material, where all the material parameters are uniform through the concrete body. This assumption is valid for macroscopic modeling. To understand the effect of aggregates on the specific heat and the thermal conductivity a mesoscopic modeling should be performed. In this kind of modeling, material parameters varies through the concrete.

The key material parameter of concrete thermomechanics is the coefficient of thermal expansion (CTE). CTE is a mechanical parameter and it has an important role in the coupling of thermal and mechanical forces. Zhou, Huang and Shu [71] developed a numerical formulation for CTE of Portland cement concrete. Moreover, Maruyama and Teramoto [51] conducted experiments under different conditions to analyze the characteristics of CTE. Although both studies claim that the CTE of normal-strength concrete has a slight decrease with respect to time, we neglect this small change and assume that CTE is constant throughout the hydration. In our model, we take CTE as $2.2 \times 10^{-5}[1/\mathrm{K}]$.

3.7.2   Mechanical Material Parameters

In this section, we give the formulation of four important mechanical material properties. These are the compressive strength, the tensile strength, the modulus of elasticity, and the Poisson's ratio. The first three equations are interrelated and the latter parameter is expressed independently.

The compressive strength, the tensile strength, and the modulus of elasticity can be described through aging. In Section 3.6, the specific equations of aging were introduced and the compressive strength is formulated as a function of the aging variable

$$f_c(\chi) = \hat{\chi} f_c^{\infty}\,.$$

39

The tensile strength $f_t(\chi) = 1.40\,(f_c(\chi)/10)^{2/3}$ and the modulus of elasticity $E_c(\chi) = 2.15 \cdot 10^4\,(f_c(\chi)/10)^{1/3}$ are nonlinearly dependent on compressive strength. For the simulations and experiments about determining these mechanical material properties, the reader is referred to [17, 45, 70, 30].

De Schutter and Taerwe [24] introduced the degree of hydration-based Poisson's ratio $\hat{\nu}(\xi)$, which is necessary to define the instant values of the bulk modulus and the shear modulus

$$\hat{\kappa}(\chi) = E_c(\chi)\,/\,3(1 - 2\hat{\nu}) \quad \text{and} \quad \hat{\mu}(\chi) = E_c(\chi)\,/\,2(1 + \hat{\nu}) \tag{3.35}$$

with the Poisson's ratio

$$\hat{\nu}(\xi) = 0.18\,\sin(\pi\xi\,/\,2) + 0.5\,\exp(-10\xi)\,. \tag{3.36}$$

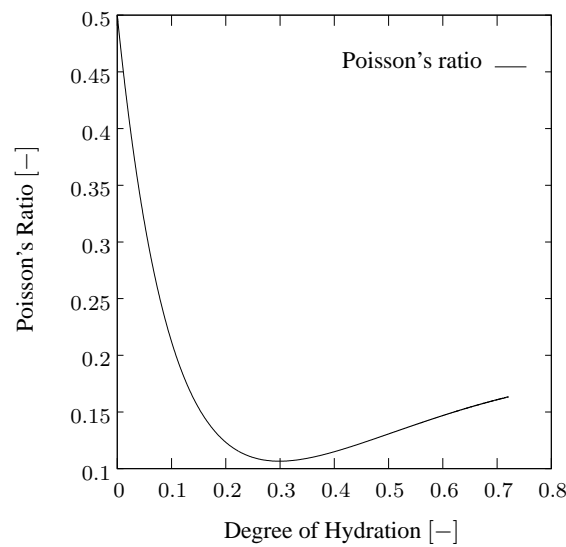The evolution of the Poisson's ratio with the degree of hydration is depicted in Figure 3.2.

Figure 3.2: Evolution of the Poisson's ratio of normal strength concrete with 20% fly ash.

CHAPTER 4

REPRESENTATIVE NUMERICAL EXAMPLES

In Chapter 2, the thermomechanics of the three-dimensional continuum has been introduced. The constitutive equations of the coupled initial boundary-value problem of early-age concrete thermomechanics within the framework of Theory of Reactive Porous Media have been derived in Chapter 3. The aim of this chapter is to demonstrate the potential of the proposed constitutive model through representative numerical examples where the numerically obtained results are contrasted with the experimental findings taken from literature.

For this purpose, three numerical examples are considered. The first example is concerned with the simulations of the results presented in Cervera, Oliver and Prato [17]. The evolution of temperature, the change of the chemical affinity, and the evolution of compressive strength are modeled at a local material point. In these simulations, the material parameters of the proposed model are identified for the distinct concrete types. In the second numerical example, experimental results in Ilısu Dam Report [13] are simulated. In this report, the evolution of adiabatic temperature and compressive strength is given for a cubic concrete specimen. The experiments have been performed to understand the characteristics of concrete, which is used in Ilısu Dam. The third example is concerned with the simulation of the thermomechanically coupled behavior of mass concrete structures. The stress and temperature distributions within the mass concrete structure are analyzed. Also, a damage study is performed to predict the potential risky areas of cracking in the structure.

4.1 Local Analyses of Experimental Results

This example deals with the temperature increase and the change of chemical affinity of normal-strength concrete with a water-cement ratio of 0.45 under adiabatic condition. The temperature-time and the chemical affinity-degree of hydration curves are depicted in Figures 4.1a and 4.1b, respectively. In these figures, the computational results, which are obtained by the proposed constitutive equations, are compared with the experimental results in Bentz, Waller and de Larrard [15]. The material parameters of the proposed model are identified and listed in the third column of Table 4.1, entitled Figure 4.1. The final value of the degree of hydration is calculated by using (3.21). In the beginning of hydration, the rate of hydration is slow. After the activation threshold is exceeded, the hydration process accelerates. The rapid increase of temperature under adiabatic conditions increases the rate of hydration. When the chemical affinity reachs its peak value, the rate of hydration slows down. As a result of this, the rate of temperature increase decreases, and because of the adiabatic condition, temperature converges to its steady-state value $\sim 82°$C.
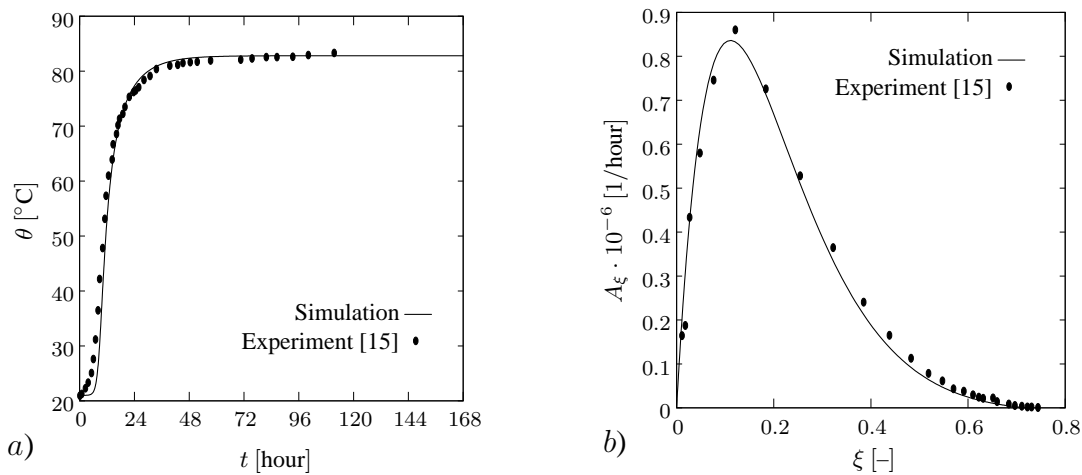
Figure 4.1: a) The evolution of temperature and b) the change of the chemical affinity of normal strength concrete with 45% water-cement ratio during concrete hardening under adiabatic conditions. The experimental results are taken from the study of Bentz, Waller and Larrard [15].

In order to investigate effect of the silica fume on the chemomechanics of concrete hardening, an adiabatic experiment analogous to the preceding example on 20% silica

42

fume containing concrete mixture with 0.45 water-cement is considered [15]. For this mixture, the temperature-time and the chemical affinity-degree of hydration curves are depicted along with the simulated results in Figures 4.2a and 4.2b, respectively. The material parameters which are used to obtain the numerical results of this example are given in Table 4.1 in the fourth column, entitled Figure 4.2.
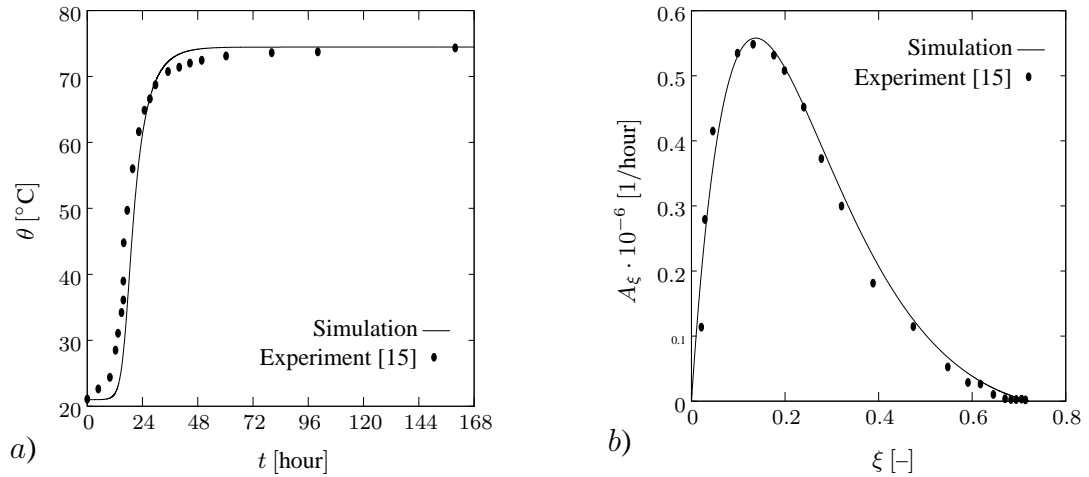
Figure 4.2: a) The evolution of temperature and b) the change of the chemical affinity of high performance concrete, which has 45% water-cement ratio and 20% silica fume, during concrete hardening under adiabatic conditions. The experimental results are taken from the study of Bentz, Waller and Larrard [15].

As we compare the curves in Figure 4.1 and Figure 4.2, it can be observed that they differ from each other considerably. This holds especially for the chemical affinity-degree of hydration curves. Silica fume addition increases the time length of low rate of hydration stage in the early ages of hydration and decreases the temperature increase, the rate of temperature increase and the chemical affinity. As it can be observed from the comparison of the obtained simulation results with the experimental findings in Figures 4.1 and 4.2, the constitutive model based on the Theory of Reactive Porous Media can favorably estimate the experimental results. However, at the first 15-20 hours, there is a lag between the experimental and simulated results. The temperature evolution equation for the adiabatic cases (3.26) explains this lag. The temperature evolution is directly influenced by the viscosity and in the theory of reactive porous media, viscosity represents the diffusion of water through the hydrated layers of concrete structure. In Figures 4.1 and 4.2, there is no temperature increase

43

until the occurance of setting.

The evolution of temperature and the chemical affinity are influenced by material parameters. To observe the effect of material parameters on the curves of Figure 4.1 and 4.2, a sensitivity study is conducted and the results are depicted in Figures 4.3–4.9. This study is peformed for c, Q_ξ, E_a/R, $k_{\xi_\infty}/\eta_{\xi_0}$, A_{ξ_0}/k_ξ, ξ_∞, and η. During the sensitivity analysis, one material parameter changes and other parameters remain same. The base values of parameters are taken from the Table 4.1, fourth column. In the figures, the sense of the arrow indicates the increase in the corresponding material.

a) *b)*
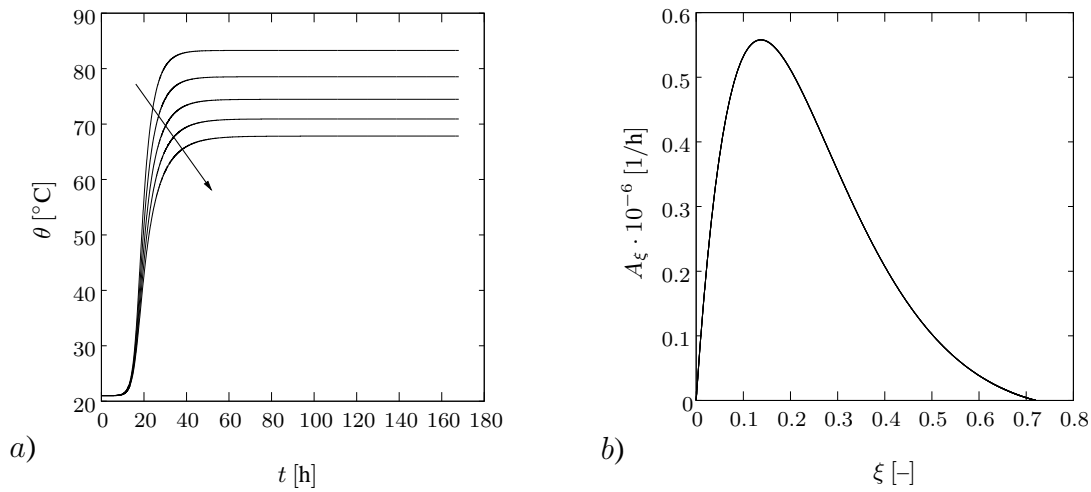
Figure 4.3: Sensitivity analysis of *a)* temperature and *b)* chemical affinity for the different values of $c = \{1, 2, 3, 4, 5\} \times 10^6$ [J/m^{3}K].

Specific heat capacity is an important thermal material parameter. In Figure 4.3, for the lower values of of specific heat, the temperature of concrete increases. Q_ξ enters the adiabatic temperature increase formulation as an internal heat source. In Figure 4.4, when heat source increases, the temperature increases. In Figure 4.5, the universal gas constant decreases the evolution of the degree of hydration and increase in the constant causes a reduction in temperature. $k_{\xi_\infty}/\eta_{\xi_0}$ is a multiplier of the degree of hydration rate. When it incrases, the change of chemical affinity and temperature also increases in Figure 4.6.

A_{ξ_0}/k_ξ has a very low influence on both temperature and chemical affinity in Figure 4.7. In the evolution equation of the degree of hydration (3.24), A_{ξ_0}/k_ξ is divided to ξ_∞. It does not effect the degree of hydration directly.

44
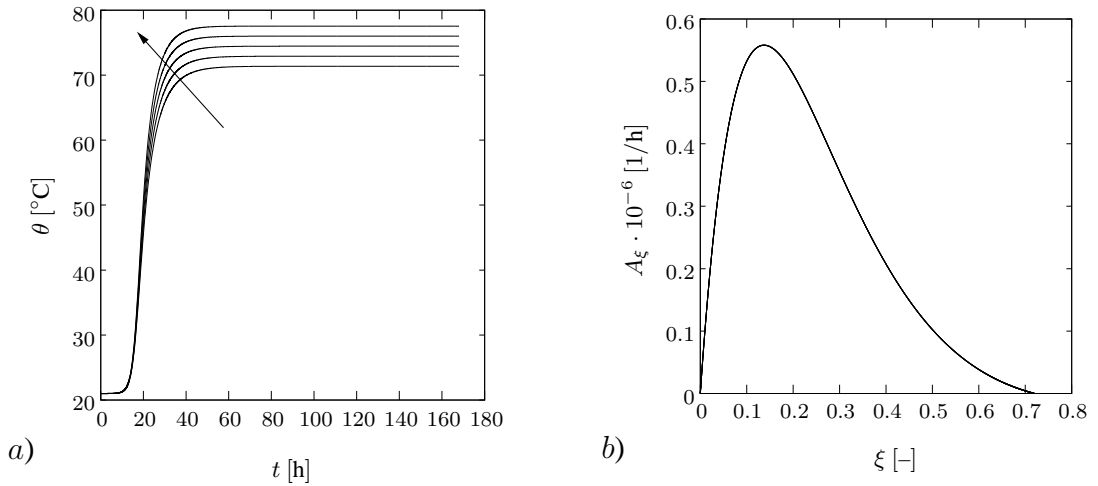
Figure 4.4: Sensitivity analysis of a) temperature and b) chemical affinity for the different values of $Q_\xi = \{1.63, 1.68, 1.73, 1.78, 1.83\} \times 10^8$ [J/m^3].

Figure 4.5: Sensitivity analysis of a) temperature and b) chemical affinity for the different values of $E_a/R = \{4.5, 4.7, 4.9, 5.1, 5.30\} \times 10^3$ [-].

The ultimate value of the degree of hydration ξ_∞ has a big influence on both the degree of hydration and the chemical affinity. In Figure 4.8, increase in the ξ_∞ results with an increase in temperature and the change of chemical affinity.

In the time - temperature curve of Figure 4.9, viscosity does not effect the ultimate value of temperature, but determines the slope of the curve. If viscosity decreases, concrete reaches the ultimate temperature value faster. For the change of chemical affinity, viscosity has an important influence on the value of chemical affinity. In-

45
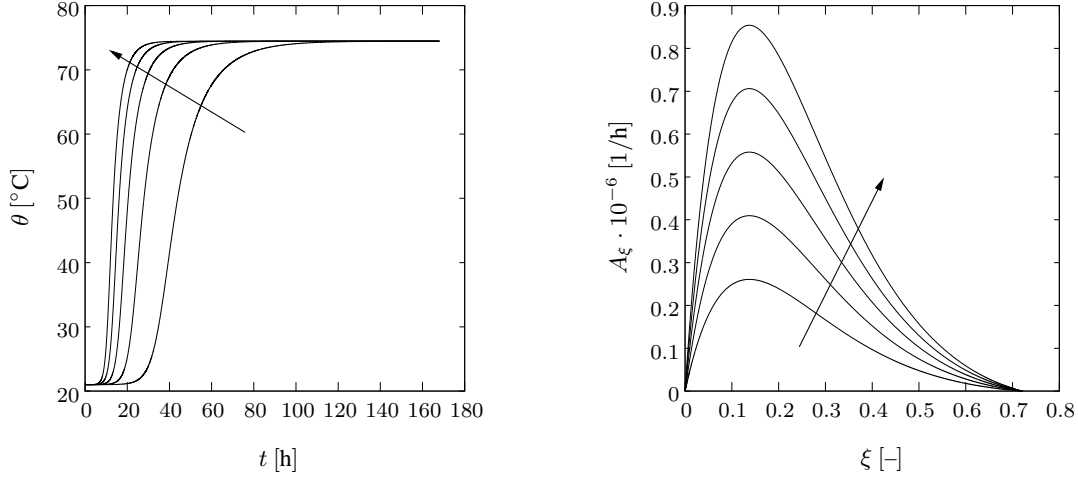
Figure 4.6: Sensitivity analysis of a) temperature and b) chemical affinity for the different values of $k_{\xi_\infty}/\eta_{\xi_0} = \{0.07, 0.11, 1.15, 0.19, 0.23\} \times 10^8$ [1/h].
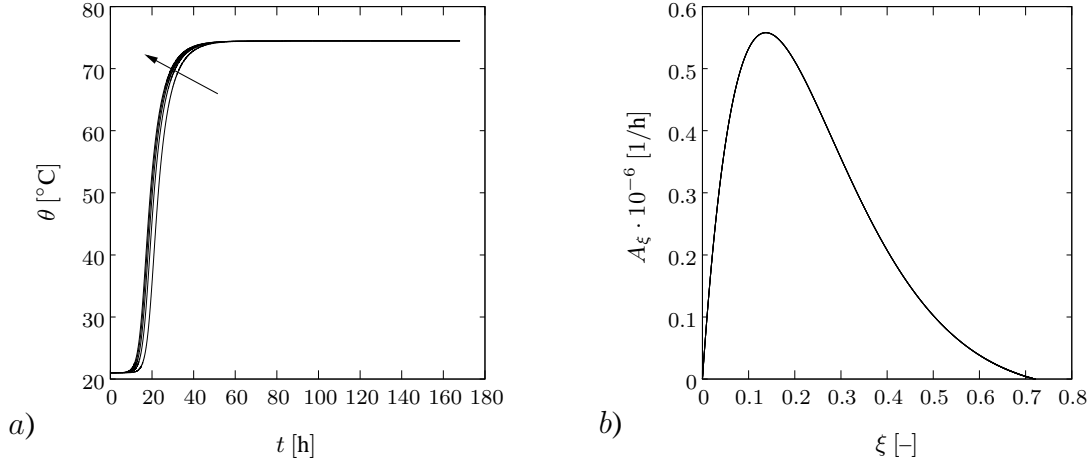
Figure 4.7: Sensitivity analysis of a) temperature and b) chemical affinity for the different values of $A_{\xi_0}/k_\xi = \{0.10, 2.60, 5.10, 7.60, 10.10\} \times 10^{-5}$ [−].

crease in viscosity decreases the change of chemical affinity.

The last study of this example is conducted with the goal of determining the effect of temperature on the concrete's rate of strength gain and the ultimate strength of concrete at the end of the hydration process at different temperature values under isothermal conditions. We recall the rate of hydration is defined by (3.7)

$$\dot{\xi} = \frac{\hat{A}_\xi}{\hat{\eta}_\xi} \exp\left(-\frac{E_a}{R\theta}\right) .$$

This formulation represents that hydration is a thermally activated process and at low

46
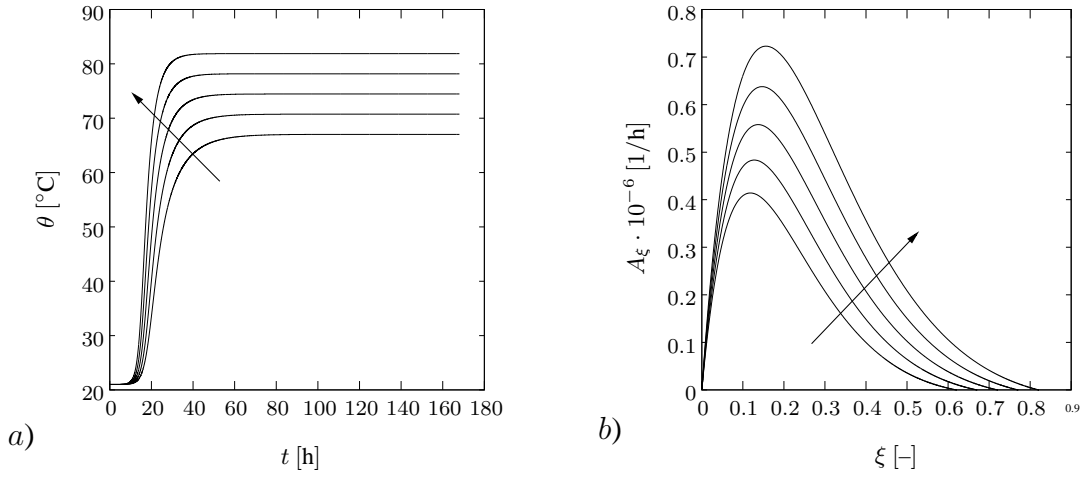
Figure 4.8: Sensitivity analysis of a) temperature and b) chemical affinity for the different values of $\xi_\infty = \{0.62, 0.67, 0.72, 0.77, 0.82\}$ $[-]$.
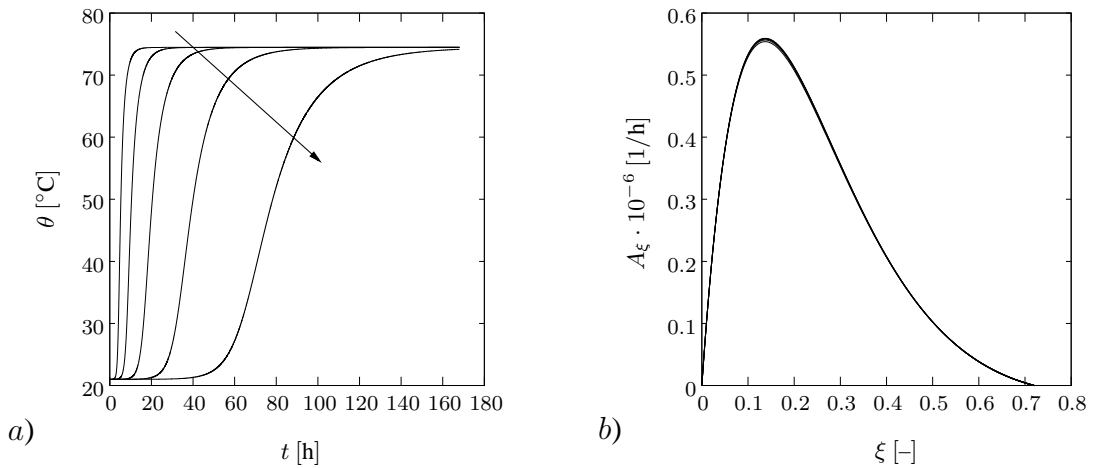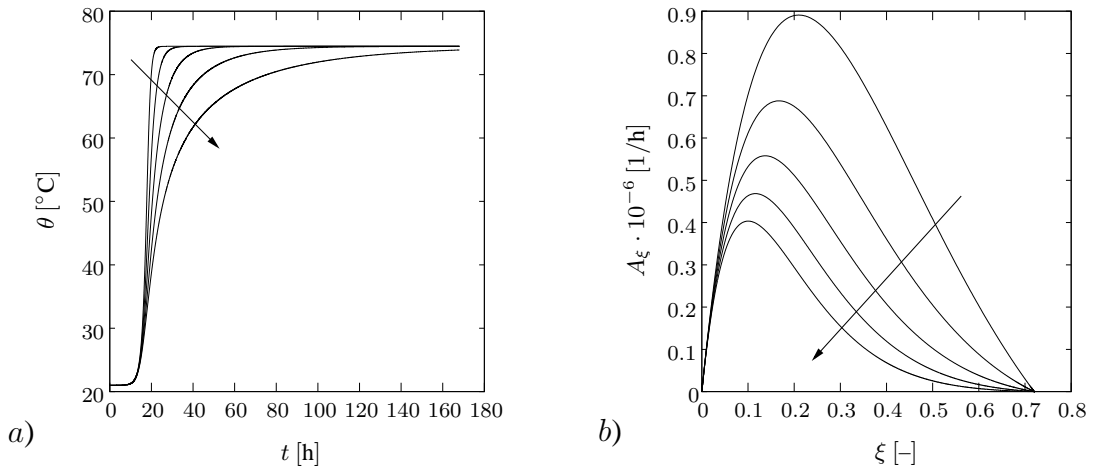

Figure 4.9: Sensitivity analysis of a) temperature and b) chemical affinity for the different values of $\eta = \{2, 3, 4, 5, 6\}$ $[-]$.

temperatures, the rate of hydration slows down. As a result of this, hydration products are formed slowly and this event helps water to diffuse inside the cement paste more easily and react with unhydrated cement particles more homogenously. Therefore, concrete hydrated at lower temperatures is expected to have a higher amount of hydrated products and higher strength performance by the help of regularity in its microstructure. However, hydration at higher temperatures, hydrated products form rapidly and this may cease the diffusion of water in the cement paste. As a result of this, the rapidly formed products make concrete gain a higher initial strength but

47

Table 4.1: Material Parameter Coefficients of Simulations

Parameter	Unit	Figure 4.1	Figure 4.2	Figure 4.10
c	$[10^6 \ \text{J/m}^3\text{K}]$	2.33	2.33	2.07
θ_0	[K]	294	294	294
Q_ξ	$[10^8 \ \text{J/m}^3]$	2.02	1.73	1.25
ξ_∞	[-]	0.72	0.72	0.75
$k_{\xi_\infty}/\eta_{\xi_0}$	$[10^8 \ \text{1/hour}]$	0.28	0.15	0.32
η	[-]	5.30	4.00	6.50
A_{ξ_0}/k_ξ	$[10^{-5}\text{-}]$	0.50	0.50	1.00
E_a/R	$[10^3\text{-}]$	4.92	4.90	5.00
f_c^∞	[MPa]	-	-	58.0
θ_r	[K]	-	-	293
$\theta_{\max}$	[K]	-	-	393
n_θ	[K]	-	-	0.40
A_f, B_f	[-]	-	-	0.47, 1.16

because of limited diffusibility, an ultimate strength of concrete becomes lower than that of the concrete hydrated at a lower temperatures. This effect has also been discussed by Mehta and Monteiro [52] who explain that concrete cured in summer or in a tropical climate can be expected to have a higher early strength but a lower ultimate strength than the same concrete cured in winter or in a colder climate.

Kjellsen and Detwiler [41] carried out several experiments to investigate the effect of temperature on the ultimate strength of concrete under isothermal conditions. Figure 4.10 shows the correlation of Kjellsen and Detwiler's study and the proposed model. The material parameters, that are used to obtain the simulation results associated with these experimental results are listed in the column entitled Figure 4.10 in Table 4.1.

4.2 Ilısu Dam Experiments

As of 2011, hydroelectric dams provided the 11% of total primary energy production in Turkey and they are a valuable energy source for Turkey's energy production [26]. Especially over the last decade, dam construction has gained importance and several world wide known dams like Deriner Dam, Ilısu Dam, Yusufeli Dam to mention a
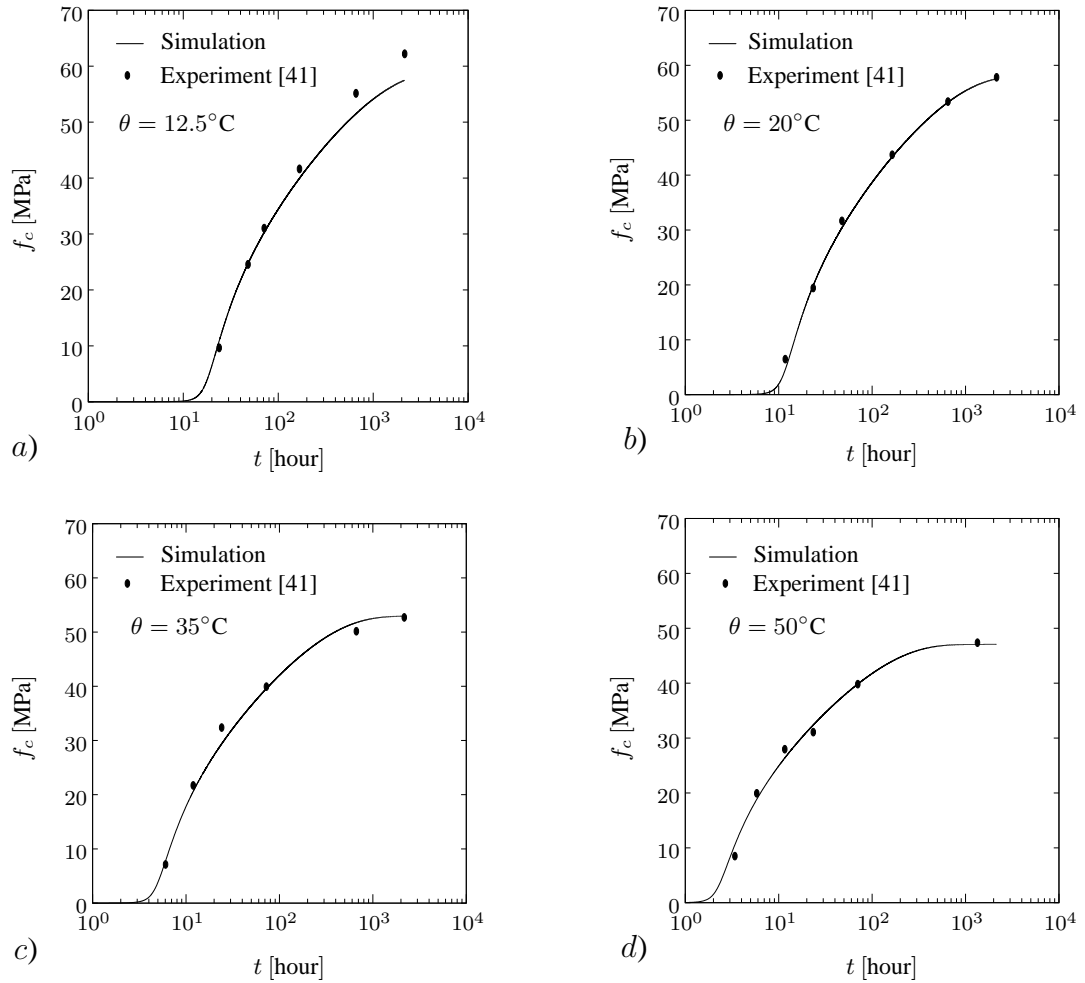
Figure 4.10: The evolution of compressive strength of hardening concrete at different temperatures under isothermal conditions. The experimental results are taken from the study by Kjellsen and Detwiler [41].

few, started to be built. Ilısu Hydroelectric Dam is located in the south-eastern region of Turkey and it has been built on the Dicle River. The area has a hot and arid climate and its annual mean ambient temperature value is $16°C$. The construction of the Ilısu Dam has been carried out by the 16th Division of the General Directorate of State Hydraulic Works (SHW).

Ilısu Dam is a front-face concrete-covered rock-filled-type dam. In this project, concrete is used for the construction of the spillway and it is considered to be mass concrete because of its large dimensions. At the construction site, various experiments are conducted in order to investigate the durability issues of mass concrete

49

[13]. These experiments cover:

1. Determination of heat of cement hydration

2. Adiabatic temperature increase estimation of concrete

3. Compressive strength tests for 7-, 28-, 90-day old concrete

First, by using the rate of heat liberation measured by isothermal calorimetry, the numerical thermal analysis of the temperature distribution in a cubic concrete sample is carried out. This distribution gives us information about the maximum and minimum temperature values and the temperature gradient in the sample. Having the temperature field estimated favorably well, the mechanical properties and the evolution of the principal stresses in the sample are analyzed.

The above-mentioned experiments were performed with the main cementitious material CEM II/A-M type cement from Mardin Cement Factory and other mineral supplementary material is F type fly ash. CEM II/A-M is a Portland composite cement and its specific gravity is 3070 kg/m^3 [64]. The other cementitious material, F-type fly ash, is obtained from the Sugözü Thermal Power Plant and its specific gravity is 2310 kg/m^3 [39].

In Table 4.2, the material parameter coefficients for the experiments in Section 4.2 and 4.3 are listed.

4.2.1   Heat of Hydration

In order to determine how much heat will be released by concrete during hydration, one needs to know the rate of heat liberation of the cementitious material used in concrete. For this measurement, 4.9 gram cement paste with 0.5 water-cement ratio, which includes CEM II type cement and 20% percentage F-type fly ash is prepared. This mixture is utilized in the isothermal calorimetry experiment and the measured rate of heat liberation-time curve is depicted in Figure 4.11 [13].

Control of the heat of hydration is mostly related with the chemical and physical properties of the cement. The rate of heat liberation highly depends on the cement

50

Table 4.2: Material Parameter Coefficients for the Experiments in Section 4.2 and 4.3

Parameter	Unit	Value
c_∞	$[m^2/s^2 K]$	800
ρ	$[kg/m^3]$	2628
α_t	$[10^{-5} \quad 1/K]$	2.2
θ_0	$[K]$	294
$k_{\xi_\infty}/\eta_{\xi_0}$	$[10^8 \ 1/hour]$	0.28
η	$[-]$	7.80
A_{ξ_0}/k_ξ	$[10^{-5}]$	1
ξ_∞	$[-]$	0.75
E_a/R	$[10^3-]$	5.1
$\hat{\chi}_0$	$[-]$	0
f_c^∞	$[MPa]$	42
θ_r	$[K]$	293
θ_{max}	$[K]$	373
n_θ	$[K]$	0.4
A_f, B_f	$[-]$	3, 0.21

Figure 4.11: The rate of heat liberation of cement paste measured by isothermal calorimetry. A 4.9 gram cement paste consists of CEM II/A-M (P-LL) and 20 % F-type fly ash [13].

fineness and the presence of supplementary materials. For instance, fly ash generally decreases the amount of the liberated heat during hydration.

According to Lawrence et al. [45], the rate of heat liberation in Figure 4.11 can be called as power data and it can be integrated with respect to time to obtain the thermal energy release. In this sense, Figure 4.12 represents the integrated rate of heat liberation as the heat of hydration as defined in the following formula

$$E = \int_{t=0}^{t} \mathcal{Q} \; dt \tag{4.1}$$

where E is the energy rise and $\mathcal{Q}$ denotes the power, which also enters the conservation of energy equation in (3.13) as a heat source.
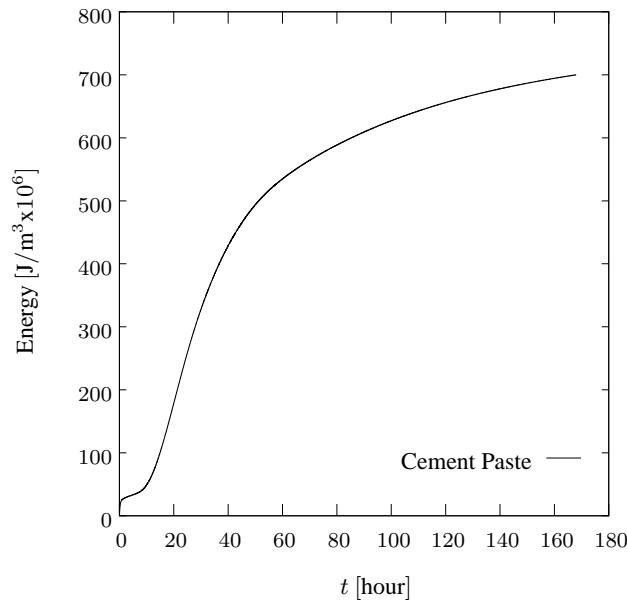
Figure 4.12: Cumulative rate of heat liberation of cement paste measured by isothermal calorimetry. A 4.9 gram cement paste consists of CEM II/A-M (P-LL) and 20% F-type fly ash [13].

4.2.2 Adiabatic Temperature Increase

For this experiment, project conductors prepared 8 different types of concrete mixtures to measure the effect of various parameters. However, as our purpose is to confirm the accuracy of our simulation's adiabatic temperature increase, we only chose

one of them. Table 4.3 shows the concrete mixture proportions of the selected mixture.

Table 4.3: Concrete Mixture Proportions

Total Cementitious (kg/m^3)	Cement (kg/m^3)	Fly Ash / Total Cementitious (%)	Water (kg/m^3)	Water / Cementitius (%)	Unit Weight (kg/m^3)
180	144	20	115	48	2628

Since most mass concrete structures include mineral supplementary materials, we preferred the concrete mixture with fly ash-total cementitious material ratio of 0.2.

There are several factors that affect the adiabatic temperature increase in concrete structures. One of them is the initial placement temperature of concrete. Initial temperature may vary in summer and winter and this may change the adiabatic temperature increase, and thereby causing a durability problem. In addition to seasonal changes, several factors may influence the initial temperature of concrete. Another factor is the coefficient of thermal conductivity of concrete. It is defined as a uniform flow of heat through a unit thickness of material between two faces subjected to a unit temperature difference during a unit time [40]. This coefficient is mostly influenced by the material characteristics of components of concrete and the local temperature. Shin et al. [62] reports that the coefficient of thermal conductivity decreases with an increase in temperature. According to the American Concrete Institute [8], the thermal conductivity coefficient of concrete can be vary in the range of 1.9-2.9 $\mathrm{W}/(\mathrm{m\,K})$.

As a result of low thermal conductivity, mass concrete structures behave like an almost adiabatic (sometimes semi-adiabatic) system. In mass concrete structures, the temperature increase in a adiabatic system can be calculated as given in (3.27).

$$\theta - \theta_0 = \frac{Q_\xi}{c} \left[\xi(t) - \xi_0 \right]$$

Here, Q_ξ is the heat source of the hardening concrete and this value can be obtained from Figure 4.12. As explained in Section 4.2.1, the heat of hydration rate was measured for a 4.9-g cement paste. However, in our model a concrete mixture is prepared and the adiabatic heat increase of concrete sample is required. Therefore, the heat

of hydration rate value of cement paste is converted for concrete sample by scaling according to the mix proportions given in Table 4.3.

A concrete cube of a 2.5 meter edge length was cast at the project site with the concrete mixture given in Table 4.3, see Figure 4.13. In order to provide a semi-adiabatic condition for concrete, the cube is covered with an insulation material named Extruded Polystrene (XPS) whose thermal conductivity ranges between 0.035 and 0.045 $W/(m\,K)$ [69]. PT100 type thermocouples are placed inside the concrete to monitor instant temperature value at those local points.

$a)$ $b)$
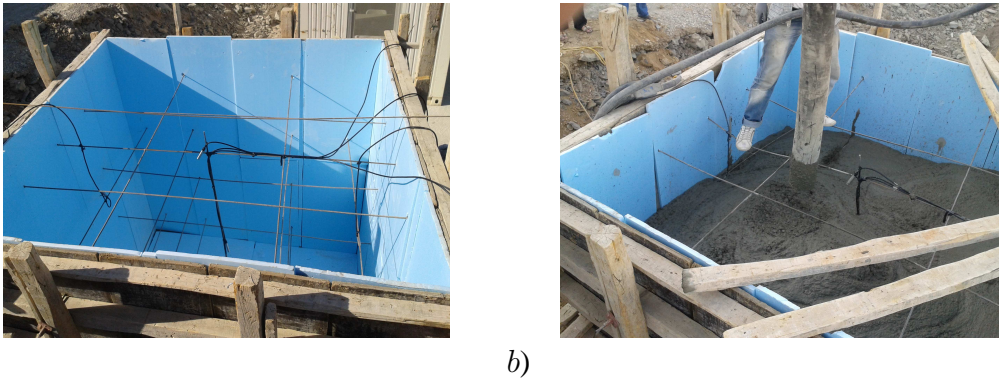
Figure 4.13: $a)$ Concrete cube isolated with XPS, $b)$ normal strength concrete is casted inside the cube [13].

A simple geometry and central cross sectional view of thermocouple locations are depicted in Figure 4.14. Three thermocouples are located in the center axis of the cube to investigate the planar temperature variations within the specimen. The other two thermocouples are used to measure the temperature changes at the sides and at the free surface of the specimen. In the finite element simulations, 15625 8-node trilinear heat transfer brick and 20-node quadratic elements are used for thermal and mechanical analysis, respectively. Convergence study is conducted during the thermal analysis.

In the numerical analyses, we use ABAQUS [1] software package which is a computer-aided engineering simulation tool of finite element analyses. ABAQUS allows one to implement his/her own constitutive model. This software enables us to indicate initial and boundary conditions and mesh the body. Using Finite Element Method (FEM), it

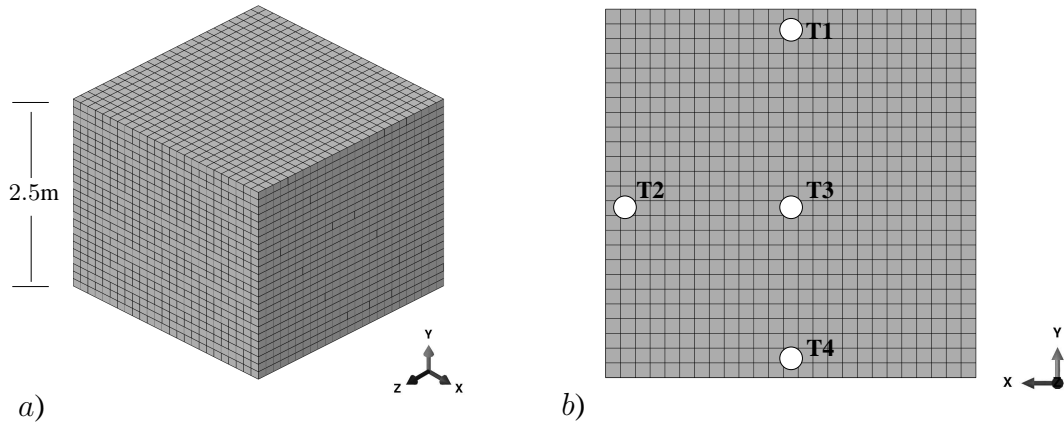Figure 4.14: a) Finite Element discretization of the cubic specimen of 2.5 m edge length into $25 \times 25 \times 25$ 8-node brick thermal elements. b) The relative locations of the thermocouples locations. The spacing between the thermocouples and the concrete surfaces is 0.1 m for all sides.

solves nonlinear initial boundary-value problems. In our case, we first create a cube and define the pre-defined material parameters. Material parameters which are given in their special forms in Section 3.7 are defined in seperate User Material (UMAT) and User Thermal Material (UMATHT) subroutines.

In the adiabatic temperature increase analysis, we created a 2.5 meter dimensioned cubic model of concrete and covered the bottom and sides with a 6 cm thickness insulation material (XPS). Thermal conductivity of concrete and XPS are 2 and 0.04 $[\mathrm{W}/(\mathrm{m\,K})]$ and the specific heat capacity of hardened concrete is defined as 850 $[\mathrm{m}^2/(\mathrm{s}^2\,\mathrm{K})]$. In the experiment, thermocouples except the centered one are placed 10 cm apart from the sides. Therefore, we mesh the cube with using 10 cm intervals to correlate the experimental and simulated results.

Table 4.4: Heat Transfer Coefficients for Different Isolation Types $[\mathrm{W}/(\mathrm{m}^2\,\mathrm{K})]$

	Top	Side	Bottom
Bofang	10	2.5	0.8
Mehta and Monteiro	11.6	2.3	-

In the adiabatic heat increase study, the main problem is to model the effect of insulator and the ambient temperature on the concrete surface. If the modeling of these

two quantities are not sufficient, then the semi-adiabatic condition of concrete might be doubtful. ABAQUS provides a feature of surface film condition to model a heat transfer coefficient. It requires a sink temperature and a film coefficient of the concrete surface. To determine this coefficient, a procedure is explained by Zhu Bofang [16] and Lee et al. [46] in detail. Mehta and Monteiro [52] give the film coefficients for different isolation environments in their book. This property is highly dependent on the wind speed. Heat transfer coefficient increases as the wind speed increases. As the experiment is conducted in Mardin, the wind speed of Mardin is obtained from the wind speed map of Turkey [7]. Moreover, soil temperature of the project site is approximately estimated from the international soil temperature map [5].

Film coefficients belong to the top, side, and bottom surfaces of concrete are listed in Table 4.4. On the top surface of concrete cube, there is not any insulator or formwork, so the ambient directly in touch with concrete surface. Wood formwork and XPS insulation material protect the concrete face from the ambient at the side surfaces. In the bottom surface, wood formwork and XPS interacts with soil, so the smallest coefficient is used here.

Semi-adiabatic temperature increase simulation is performed with Bofang's heat transfer coefficients. Duration of the simulations and the experiment is one week. A general view of temperature distribution in the cube is demonstrated in Figure 4.15 in a cross sectional view.
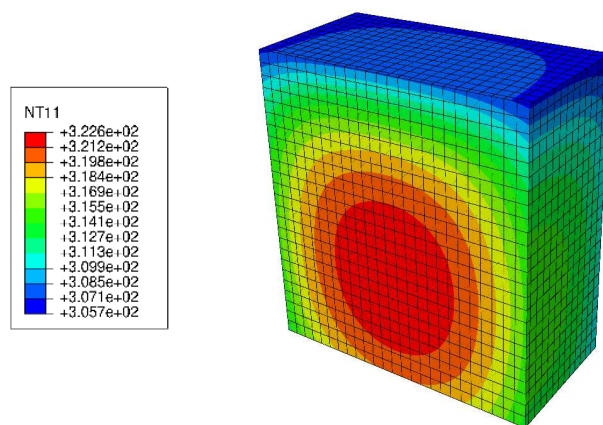

Figure 4.15: Simulated contour plot of temperature distribution of concrete cube in section cut view at 1.25 m.

56

This contour plot shows the temperature field in the middle section of the cube at the end of 7 days. In this plot, temperature of the bottom and the central regions looks quite similar. Another fact is that the temperature difference between the red and blue part is nearly 22 °C and this is an undesired situation according to the ACI 207.1R-96 report.

In the project site, temperature values and the thermal gradient inside the concrete element are recorded. These records are compared with the numerical findings in Figure 4.16 and a good agreement is observed. However, for the temperature of top and side thermocouples, the fluctuation begins after 50 hours. The reason of this condition is the ambient temperature. This experiment is performed in Mardin, which is very hot in the daylight and cold in the nights. T1 and T2 thermocouples are very close to the surface. So, they are highly influenced by the changing ambient temperature. In the center and bottom thermocouples, fluctuation is not observed.

4.2.3 Compressive Strength

The proposed coupled thermomechanical model is verified on thermal field with the adiabatic temperature increase test described in the last section. In this section, the mechanical verification of the model is conducted. In this manner, the compressive strength of the cast concrete is compared with the simulation results and good match is observed. Compressive strength of concrete is measured on 7, 28, and 90 days. Also, the strength at 180 day is estimated. A local MATLAB code is written to calculate the compressive strength of concrete by using (3.28). Recall the compressive strength equation based on aging variable is

$$f_c(\chi) = \hat{\chi} f_c^\infty \,.$$

Table 4.5 shows the compressive strength experiment result value of the concrete cube for 7, 28, 90 and 180 days.

The proposed constitutive equations in Chapter 3 are solved iteratively through the backward Euler Algorithm and compressive strength of concrete is obtained. The simulated compressive strength curve is contrasted with the experimental results in Figure 4.17.
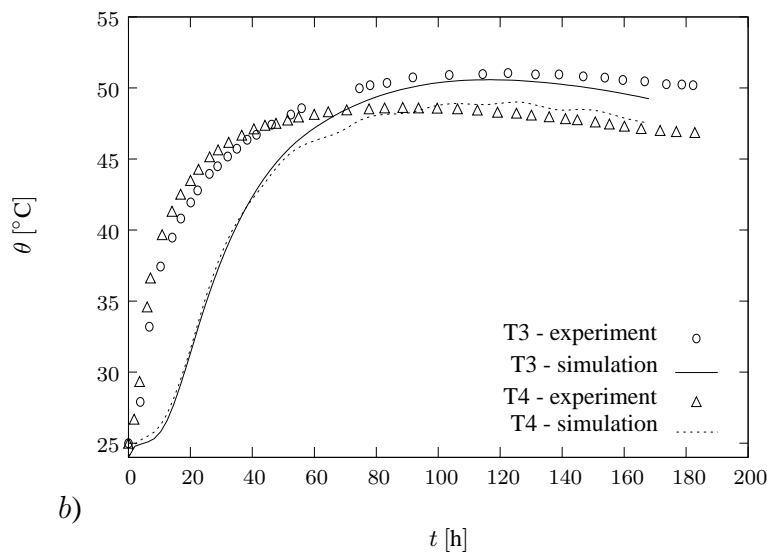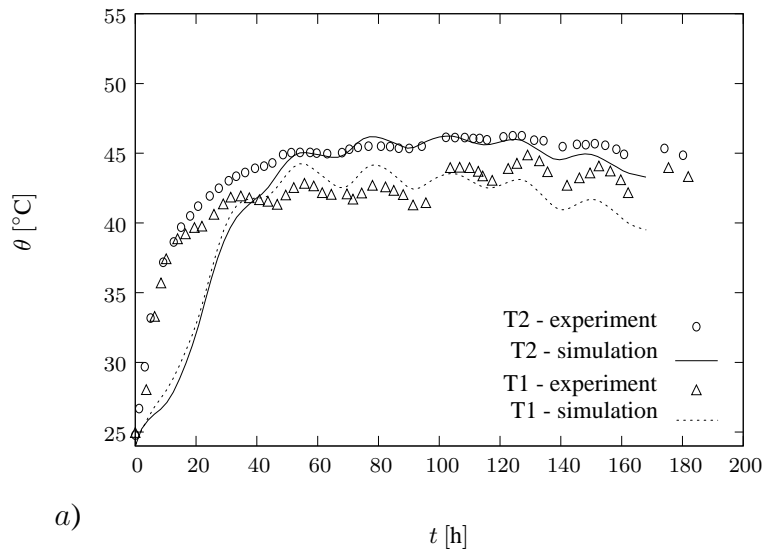
Figure 4.16: Comparison of simulation and experimental results, recorded at different thermocouples. Temperature curves of experiments and the corresponding simulations are plotted in a) for T1 and T2, in b) for T3 and T4. Experiment results are taken from the study of SHW 16th Division [13].

In Figure 4.18, principle stress distributions of the concrete cube is given. According to Figure 4.18, maximum tensile stress is concentrated at the corners and the compressive stress is at the center of the cube. This cubic concrete is solved thermomechanically by using 121 mesh elements. A 20-node thermally coupled brick element is used in finite element solution of the problem.

Figure 4.17: Compressive strength of concrete with 20 % fly ash at 7, 28, 90 and 180 days.

In this section, we checked the accuracy of our novel constitutive model for the thermal field. In the first subsection, isothermal calorimet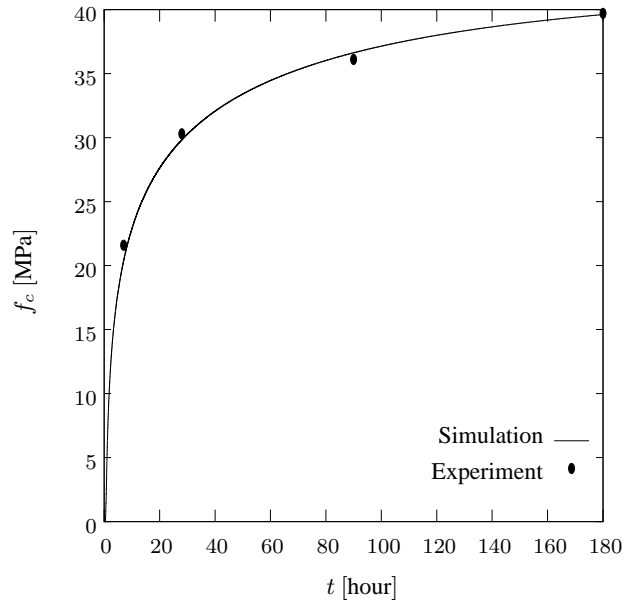ry experiment is done to obtain the heat of hydration rate and the integrated hydration heat. This heat of hydration rate enters the conservation of energy equation as a heat source and so far, we managed to model the adiabatic heat increase for the concrete cube which is isolated with a insulation material. In this study, our model and the experimental findings present a good match. In the last experiment, evolution of compressive strength of our constitutive model is verified with the concrete cube's results. Thus, thermal and aging equations of the model are confirmed.

Table 4.5: Compressive Strength of Concrete Cube for 7, 28, 90 and 180 days [MPa]

Days	Compressive Strength
7	21.6
28	30.3
90	36.1
180	39.7

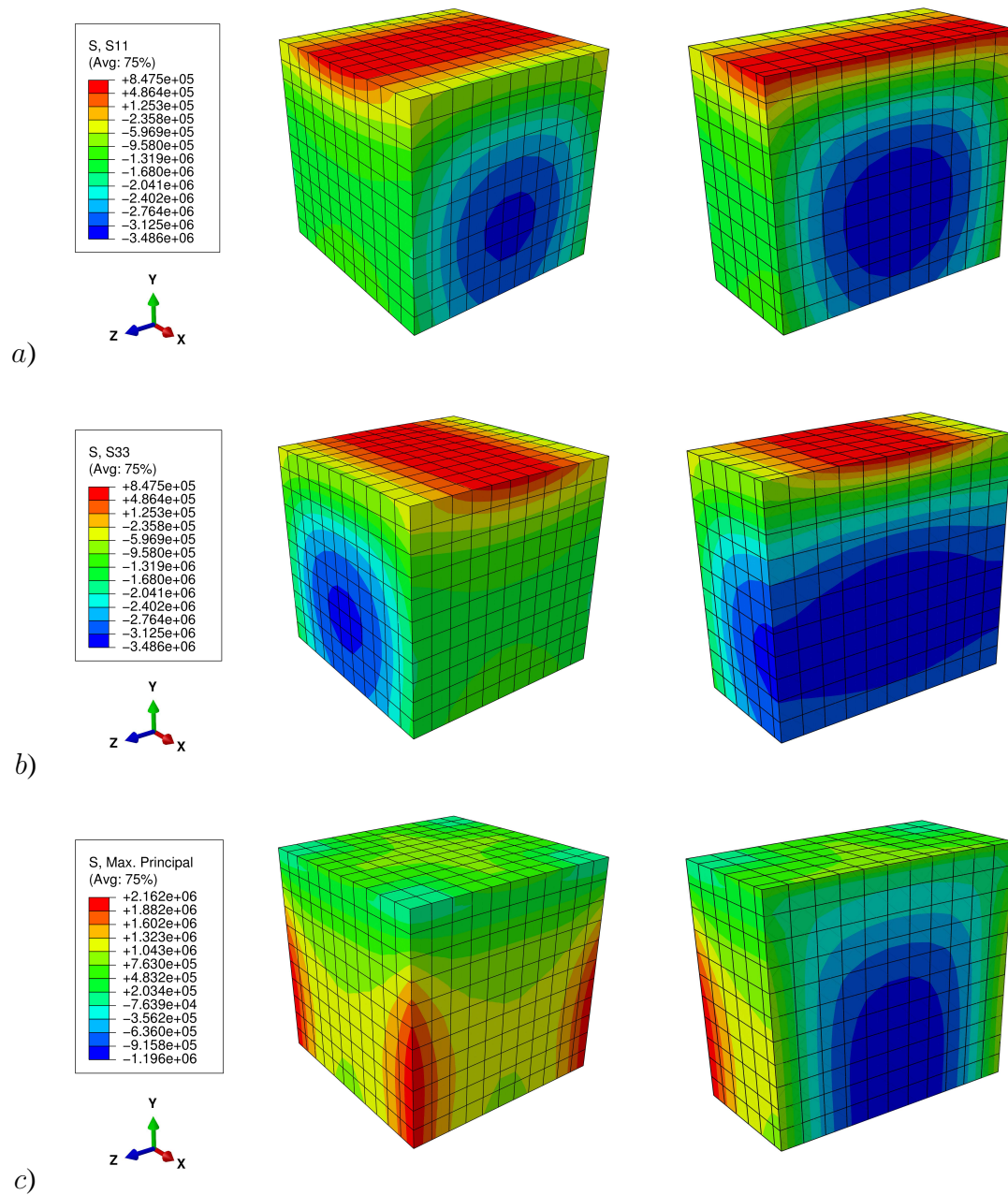Figure 4.18: Stresses in x-direction, z-direction and the maximum principal stress distributions are given in a), b) and c) with their normal (left) and section cut (right) views, respectively.

4.3 Thermomechanical Analyses of a Mass Concrete Structure

The aim of this example is to conduct a predictive thermomechanical analysis of a mass concrete structure by using the proposed coupled model and the model param-

eters identified in the preceding section based on the concrete mix used in Ilısu Dam.

In a mass concrete, the effects concerned with the temperature gradient development and the stress concentrations observed in the simple cube of previous example become more pronounced. Since the interior region of concrete stays hot and the surface is under the influence of ambient temperature and wind, the hot region tends to expand and the outer region tends to shrink. These uneven thermal volume changes in concrete structures leads to tensile stress concentrations because of external restraints [42].

In order to reveal the characteristics of induced stresses, we model a large volumed mass concrete example. To this end, the geometry of Deriner Dam is created in ABAQUS CAE (Computer Aided Engineering) platform, see Figure 4.19. Deriner Dam has a double curvature geometry and the height of dam is 249 m with the 62 m base and 34 m top depth.
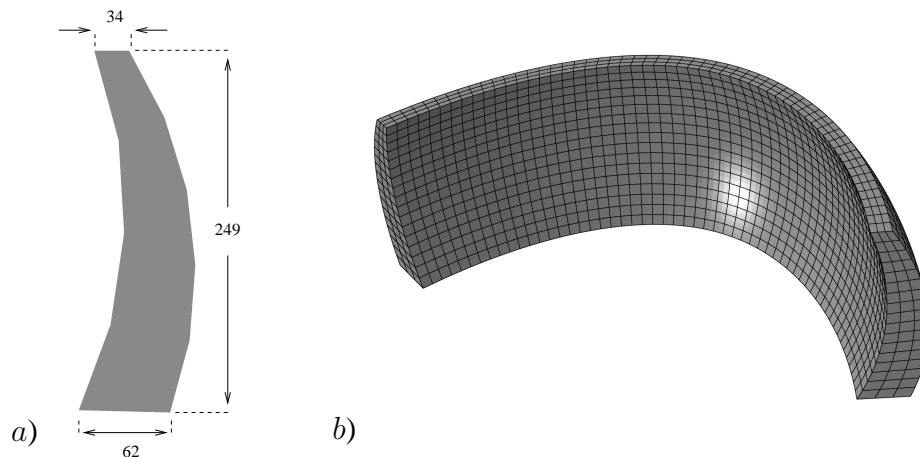
Figure 4.19: a) Section view sketch and b) mesh discretization of Deriner Dam. Dimensions are given in meters.

In the Deriner Dam simulation, the bottom surface and the two side surfaces are mechanically restrained. Also, initial temperature condition of the whole model is set as 21 °C. The same procedure and the material parameters of the concrete cube example is applied to this simulation. At the end of the analysis, the maximum principal stress and temperature distribution of the dam are obtained and presented in Figure 4.20. It is also possible to observe the volume change of the dam from these figures.
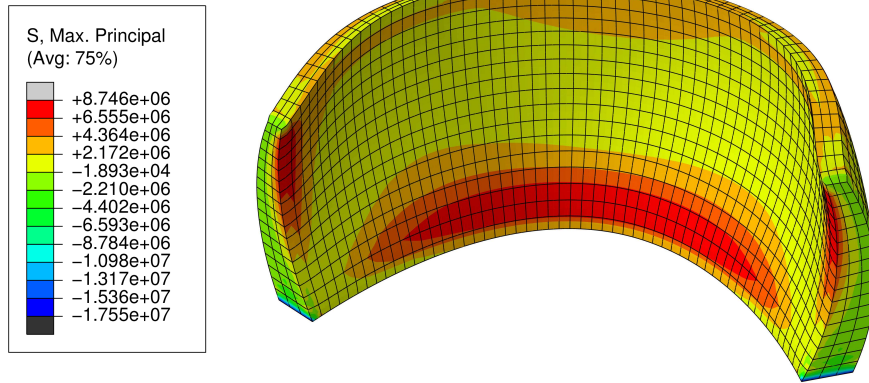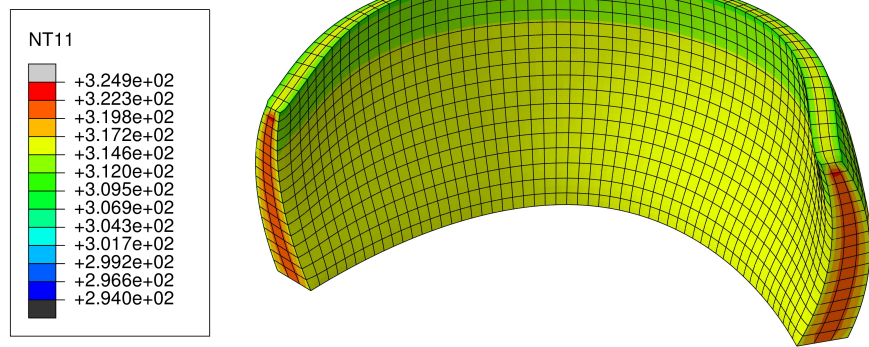
Figure 4.20: Distribution of a) maximum principal stress [MPa] and b) temperature [K] of Deriner Dam.

The thermal boundary conditions make the front and back surfaces of the dam cooler. As shown in Figure 4.20b, the maximum temperature occurs in the middle of the section. This condition creates a thermal gradient between the center and the surface of the dam. Because of this gradient and the degree of freedoms of the structure, the maximum principle stress is occured in the interior face of the dam. In order to predict the potential of cracking, the degree of damage is defined as

$$\delta = \frac{\boldsymbol{\sigma}_{max} - f_t}{f_t} \tag{4.2}$$

The aim of the degree of damage is to indicate the locations where the maximum principle stress is greater than the tensile strength. For Deriner Dam model, the degree of damage distribution is depicted in Figure 4.21.

Figure 4.21 is plotted for only the positive values of the degree of damage. There-
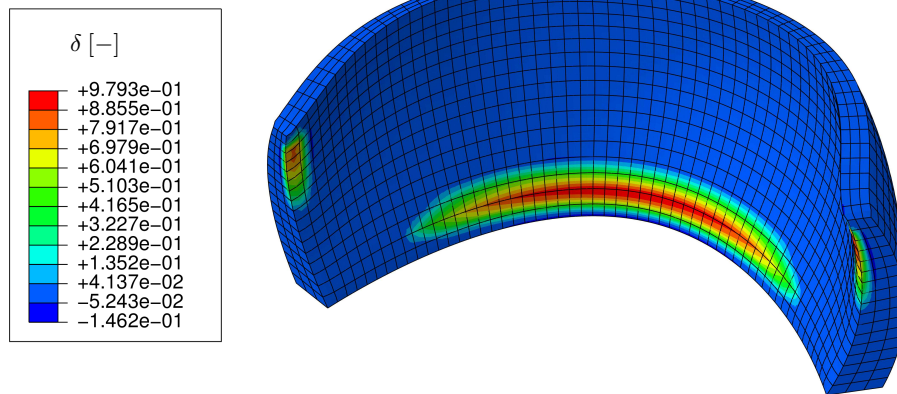
Figure 4.21: Distribution of the degree of damage. This figure is depicted only for the positive values of degree of damage. Colored regions have potential for cracking.

fore, the colored parts of the dam can be indicated as the areas of potential cracking region.

CHAPTER 5

CONCLUDING REMARKS

In this thesis, we have presented a computational three-dimensional early-age concrete hardening model in thermodynamical framework to simulate the cement hydration for the hardening mass concrete structures. The simulation results are shown to agree with the experimental results for these kind of structures.

Before advancing the new model, fundamentals of geometrically linear continuum mechanics are introduced for the formulation of a general coupled thermomechanical problem. Numerical application of a coupled thermomechanical problem is accomplished with monolithic coupling algorithm. Then, constitutive equations of concrete thermomechanics are given.

To better understand the behavior of early-age concrete structures, thermal and mechanical analyses are achieved. In the thermal analysis, temperature development of concrete structure is obtained and the local temperature values are stored as internal variable. The mechanical analysis captures structural behavior of early-age concrete and computes stress components using temperature field from the thermal analysis as a body heat source.

Numerical simulations show that the proposed model has a good agreement with the selected experimental results. In order to achieve this agreement, numerous thermal and mechanical comparisons are implemented. Temperature and chemical affinity evolutions are predicted correctly. The degree of aging forms the fundamental equations for the evolution of mechanical properties of concrete. Deriner Dam analysis confirms that the stresses developing in the early-age of mass concrete plays a signif-

icant role on the durability of mass concrete structure. Heat of hydration rate enters the coupled model as a heat source and it becomes two laods with gravity, which applied on the structure and coarsely predict the real situation.

In the literature, there are several studies on modeling coupled thermomechanical behavior of early-age concrete and cement hydration. Besides, modeling of mass concrete structures and stress estimation for concrete gravity and RCC dams have been investigated by numerous researchers. However, there are only few studies on modeling the behavior of cracking and developing a coupled thermomechanical algorithm for mass concrete structures. Our research can be further extended to model several durability and stability issues of early-age or hardened concrete. Besides, investigation of the creep and shrinkage effect on change of material parameters can be a next step for this work. In addition to the durability study, effect of aggregates on specific heat and thermal conductivity can be a possible outlook. In this study, concrete is assumed as a homogenous material and the material parameters are assumed for the whole concrete body. To investigate the effect of aggregates, concrete can be modeled as a heterogenous material. Also, a multiphase porous media theory can be followed. In order to obtain more realistic results and use our model to predict the potential risky regions of mass concrete structures, the next step is to make our model to have the realistic boundary conditions and include a crack propogation algorithm.

REFERENCES

[1] ABAQUS. http://www.3ds.com/products-services/simulia/products/abaqus/. Last visited on January 2015.

[2] Deriner Barajı. http://www.atalaysondajmak.com/referanslarimiz. Last visited on February 2015.

[3] Mass Concrete Foundation. http://carrasquilloassociates.com/projects.html?p=20. Last visited on February 2015.

[4] Raw Science. http://www.rawscience.tv/san-onofre-plant-will-cost-4-billion-and-take-20-years-to-dismantle/. Last visited on February 2015.

[5] Soil Temperature Regimes Map. http://www.nrcs.usda.gov/wps/portal/nrcs/soil/. Last visited on January 2015.

[6] Subsea World News. http://subseaworldnews.com/2012/09/06/norway-emas-amc-inks-troll-subsea-power-cables-deal/. Last visited on February 2015.

[7] Yeni ve Yenilenebilir Enerji. http://www.mgm.gov.tr/arastirma/yenilenebilir-enerji.aspx?s=ruzgaratlasi. Last visited on December 2014.

[8] Mass Concrete (ACI 207.1R-96). Technical report, American Concrete Institute, 1997.

[9] Temperature Control of Mass Concrete for Dams - Guidelines (ICS 93.160). Technical report, Bureau of Indian Standards, 1999.

[10] Cement and Concrete Terminology (ACI 116.R-00). Technical report, American Concrete Institute, 2000.

[11] Standard Terminology Relating to Concrete and Concrete Aggregates. Technical report, American Society for Testing and Materials, 2006.

[12] Standard Specification for Portland Cement. Technical report, American Society for Testing and Materials, 2012.

[13] 16th Division of State Hydraulic Works. Ilısu Barajı ve HES Projesi Dolusavak Yapısı Kütle Betonu Tasarımları Teknik Raporu. Technical report, General Directorate of State Hydraulic Works, 2012.

[14] L. Bennethum and J. Cushman. Multiscale, hybrid mixture theory for swelling systems - I: Balance laws. *International Journal of Engineering Science*, 34(2):125–145, 1996.

[15] D. P. Bentz, V. Waller, and F. de Larrard. Prediction of Adiabatic Temperature Rise in Conventional and High-Performance Concretes Using a 3-D Microstructural Model. *Cement and Concrete Research*, 28(2):285–297, 1998.

[16] Z. Bofang. *Thermal Stresses and Temperature Control of Mass Concrete*. Butterworth-Heinemann, New York, 1st edition, 2013.

[17] M. Cervera, J. Oliver, and T. Prato. Thermo-chemo-mechanical model for concrete. I: Hydration and aging. *Journal of Engineering Mechanics*, 125:1018–1027, 1999.

[18] M. Cervera, J. Oliver, and T. Prato. Simulation of construction of RCC dams. I: Temperature and aging. *Journal of Structural Engineering*, 126(9):1053–1061, 2000.

[19] B. D. Coleman and M. E. Gurtin. Thermodynamics with internal state variables. *Journal of Chemical Physics*, 47:597–613, 1967.

[20] O. Coussy. *Mechanics of Porous Continua*. Wiley, New York, 1995.

[21] G. De Schutter. Finite element simulation of thermal cracking in massive hardening concrete elements using degree of hydration based material laws. *Computers and Structures*, 80(27-30):2035–2042, 2002.

[22] G. De Schutter and L. Taerwe. General hydration model for portland cement and blast furnace slag cement. *Cement and Concrete Research*, 25(3):593–604, 1995.

[23] G. De Schutter and L. Taerwe. Specific heat and thermal diffusivity of hardening concrete. *Magazine of Concrete Research*, 47(172):203–208, 1995.

[24] G. De Schutter and L. Taerwe. Degree of hydration-based description of mechanical properties of early age concrete. *Materials and Structures*, 29:335–344, 1996.

[25] T. Dolen. Advances in Mass Concrete Technology - The Hoover Dam Studies. In *Hoover Dam 75th Anniversary History Symposium*, pages 58–73, 2010.

[26] K. Erdem and M. C. Senel. Dünyada ve Türkiye'de Enerji Durumu - Genel Değerlendirme. *Mühendis ve Makina*, 54(639):32–44, 2013.

[27] T. Y. Erdoğan. *Materials of Construction*. ODTÜ Yayıncılık, Ankara, 1st edition, 2007.

[28] T. Y. Erdoğan. *Beton*. ODTÜ Yayıncılık, Ankara, 4th edition, 2014.

[29] E. Fairbairn, M. Silvoso, R. Filho, J. Alves, and N. Ebecken. Optimization of mass concrete construction using genetic algorithms. *Computers and Structures*, 82:281–299, 2004.

[30] R. Faria, M. Azenha, and J. Figueiras. Modelling of concrete at early ages: Application to an externally restrained slab. *Cement and Concrete Composites*, 28(6):572–585, 2006.

[31] D. Gawin, F. Pesavento, and B. A. Schrefler. Hygro-thermo-chemo-mechanical modelling of concrete at early ages and beyond. Part I: Hydration and hygro-thermal phenomena. *International Journal for Numerical Methods in Engineering*, 67:299–331, 2006.

[32] D. Gawin, F. Pesavento, and B. A. Schrefler. Hygro-thermo-chemo-mechanical modelling of concrete at early ages and beyond. Part II: Shrinkage and creep of concrete. *International Journal for Numerical Methods in Engineering*, 67:332–363, 2006.

[33] W. Gray and C. Miller. Thermodynamically constrained averaging theory approach for modeling flow and transport phenomena in porous medium systems: 1. Motivation and overview . *Advances in Water Resources*, 28:161–180, 2005.

[34] E. Gruyaert, N. Robeyst, and N. De Belie. Study of the hydration of Portland cement blended with blast-furnace slag by calorimetry and thermogravimetry. *Journal of Thermal Analysis and Calorimetry*, 102(3):941–951, 2010.

[35] J. Ha, Y. Jung, and Y. Cho. Thermal crack control in mass concrete structure using an automated curing system. *Automation in Construction*, 45:16–24, 2014.

[36] M. Hassanizadeh and W. G. Gray. General conservation equations for multi-phase systems: 1. Averaging procedure . *Advances in Water Resources*, 2:131–144, 1979.

[37] L. Jendele, V. Šmilauer, and J. Červenka. Multiscale hydro-thermo-mechanical model for early-age and mature concrete structures . *Advances in Engineering Software*, 72:134–146, 2014.

[38] J. H. Jeong and N. Kim. A Thermal Conductivity Model for Hydrating Concrete Pavements. *Journal of the Korean Concrete Institute*, 16(1):125–129, 2004.

[39] O. Karahan and C. D. Atiş. Sugözü Uçucu Külünün Beton Katkısı Olarak Kullanılabilirliği. In *7. Ulusal Beton Kongresi*, pages 405–416, İstanbul, 2004.

[40] J. K. Kim, K. H. Kim, and J. K. Yang. Thermal analysis of hydration heat in concrete structures with pipe-cooling system. *Computers and Structures*, 79(2):163–171, 2001.

[41] K. Kjellsen and R. Detwiler. Later Ages Strength Prediction by a Modified Maturity Method. *ACI Materials Journal*, 90(3):220–227, 1993.

[42] B. Klemczak and A. Knoppik-Wróbel. Early age thermal and shrinkage cracks in concrete structures–description of the problem. *Architecture - Civil Engineering - Environment*, 2:35–48, 2011.

[43] V. Kodur. Properties of Concrete at Elevated Temperatures. *ISRN Civil Engineering*, 2014:1–15, 2014.

[44] B. Langan, K. Weng, and M. Ward. Effect of silica fume and fly ash on heat of hydration of Portland Cement. *Cement and Concrete Research*, 32:1045–1051, 2002.

[45] A. M. Lawrence, M. Tia, C. C. Ferraro, and M. Bergin. Effect of Early Age Strength on Cracking in Mass Concrete Containing Different Supplementary Cementitious Materials: Experimental and Finite-Element Investigation. *Journal of Materials in Civil Engineering*, 24:362–372, 2012.

[46] Y. Lee, M.-S. Choi, S.-T. Yi, and J.-K. Kim. Experimental study on the convective heat transfer coefficient of early-age concrete. *Cement and Concrete Composites*, 31(1):60–71, 2009.

[47] Z. Li. *Advanced Concrete Technology*. Wiley, New York, 2011.

[48] X. Liu, Y. Duan, W. Zhou, and X. Chang. Modeling the Piped Water Cooling of a Concrete Dam Using the Heeat-Fluid Coupling Method. *Journal of Engineering Mechanics*, 139:1278–1289, 2013.

[49] G. Lixia, G. Lei, Z. Ling, and Z. Yueming. Thermal conductivity and heat transfer coefficient of concrete. *Journal of Wuhan University of Technology-Mater. Sci. Ed.*, 26(4):791–796, 2011.

[50] A. I. H. Malkawi, S. A. Mutasher, and T. J. Qiu. Thermal-Structural Modeling and Temperature Control of Roller Compacted Concrete Gravity Dam. *Journal of Performance of Constructed Facilities*, 17(4):177–187, 2003.

[51] I. Maruyama and A. Teramoto. Impact of time-dependant thermal expansion coefficient on the early-age volume changes in cement pastes. *Cement and Concrete Research*, 41(4):380–391, 2011.

[52] P. K. Mehta and P. J. M. Monteiro. *Concrete: microstructure, properties, and materials*. McGraw Hill Education, New York, 4th edition, 2014.

[53] S. Mindess and J. Young. *Concrete*. Prentice-Hall, New Jersey, 1981.

[54] A. Neville and J. Brooks. *Concrete Technology*. Pearson Education Limited, Essex, 2007.

[55] A. M. Neville. *Properties of Concrete*. Pearson Education Limited, Essex, 2011.

[56] I. Pane and W. Hansen. Investigation of blended cement hydration by isothermal calorimetry and thermal analysis. *Cement and Concrete Research*, 35(6):1155–1164, 2005.

[57] S. Pantazopoulo and R. Mills. Microstructural aspects of the mechanical response of plain concrete. *ACI Materials Journal*, 92(6):605–616, 1995.

[58] F. Pesavento, D. Gawin, and B. A. Schrefler. Modeling cementitious materials as multiphase porous media: theoretical framework and applications. *Acta Mech.*, 201:313–339, 2008.

[59] J. Ruiz, A. K. Schindler, R. Rasmussen, P. K. Nelson, and G. Chang. Concrete Temperature Modeling and Strenght Prediction Using Maturity Concepts in the FHWA HIPERPAV Software. In *Seventh International Conference on Concrete Pavements:"The use of concrete in developing long-lasting pavement solutions for the 21st century"*, pages 97–111, 2001.

[60] A. K. Schindler and K. J. Folliard. Heat of hydration models for cementitious materials. *ACI Materials Journal*, 102(1):24–33, 2005.

[61] G. Sciume. *Thermo-Hygro-Chemo-Mechanical Model of Concrete At Early Ages and Its Extension To Tumor Growth Numerical Analysis*. PhD thesis, Universita degli studi di Padova, 2013.

[62] K. Y. Shin, S. B. Kim, J. H. Kim, M. Chung, and P. S. Jung. Thermo-physical properties and transient heat transfer of concrete at elevated temperatures. *Nuclear Engineering And Design*, 212:233–241, 2002.

[63] Turkish Standards Institution. Beton agregaları. Technical report, Turkish Standards, 2009.

[64] Turkish Standards Institution. Çimento - Bölüm 1: Genel Çimentolar. Technical Report 112, Turkish Standards Institution, 2013.

[65] F.-J. Ulm and O. Coussy. Modeling of Thermochemomechanical Couplings of Concrete at Early Ages. *Journal of Engineering Mechanics*, 121(7):785–794, 1995.

[66] F.-J. Ulm and O. Coussy. Strength Growth as Chemo-Plastic Hardening in Early Age Concrete. *Journal of Engineering Mechanics*, 122(12):1123–1132, 1996.

[67] F.-J. Ulm and O. Coussy. Couplings in early-age concrete: From material modeling to structural design. *International Journal of Solids and Structures*, 35(31-32):4295–4311, 1998.

[68] B. Valentini, Y. Theiner, M. Aschaber, H. Lehar, and G. Hofstetter. Single-phase and multi-phase modeling of concrete structures . *Engineering Structures*, 47:25–34, 2013.

[69] H. Winterling and N. Sonntag. Rigid Polystyrene Foam (EPS, XPS). *Kunststoffe International*, (D):18–21, 2011.

[70] S. T. Yi, J. K. Kim, and T. K. Oh. Effect of strength and age on the stress-strain curves of concrete specimens. *Cement and Concrete Research*, 33(8):1235–1244, 2003.

[71] C. Zhou, B. Huang, and X. Shu. Micromechanical Model for Predicting Coefficient of Thermal Expansion of Concrete. *Journal of Materials in Civil Engineering*, 25:1171–1180, 2013.